years) were analyzed. The inheritance pattern was considered to be autosomal dominant in 7 (18%) eyes, autosomal recessive in 9 (23%) eyes, and sporadic in 23 (59%) eyes. None of the patients was believed to have X-linked RP. The mean logMAR (logarithm of the minimum angle of resolution) best corrected visual acuity was 0.061 ± 0.069 (1.15; Snellen equivalent). The mean radius of the central visual field with the Goldmann I4e target (average value for upper, lower, nasal, and temporal directions) was 14.8° ± 12.0°.

For controls, fmERGs were recorded from 30 age-similar normal subjects (17 men, 13 women; age, 39.4 ± 16.1 years). None had known abnormalities of the visual system, and their visual acuity was 1.0 or better.

The research was conducted in accordance with the institutional guidelines of Nagoya University and conformed to the tenets of the World Medical Association's Declaration of Helsinki. Informed consent was obtained after sufficient information was provided about the examinations.

Focal Macular Electroretinograms

The stimulating and recording systems used to record the fmERGs have been described in detail.[19,20] Briefly, an infrared fundus camera equipped with a stimulus light, background illumination, and fixation target was used. The image from the camera was fed to a television monitor, and the examiner used the monitor to maintain the stimulus on the macula.

The size of the stimulus spots was selected to be 5°, 10°, and 15°, and they were centered on the fovea. The background light was delivered to the eye from the fundus camera at a visual angle of 45°. Additional background illumination outside the central 45° produced homogeneous background illumination for nearly the entire visual field. The luminances of the white stimulus light and background light were 29.46 and 2.89 cd/m^2, respectively.

A Burian-Allen bipolar contact lens electrode was used for the recordings. This lens not only allowed a very low electrical noise, but also permitted a clear view of the fundus on the monitor during the recordings.

After the patients' pupils were fully dilated with 0.5% tropicamide and 0.5% phenylephrine hydrochloride, fmERGs were elicited by 5-Hz rectangular stimuli (100-ms light on and 100-ms light off), and 512 responses were averaged by a signal processor. With this duration, the responses to the stimulus-onset was evaluated in this study, whereas the on and off responses are inseparable with the brief-flash stimuli that are widely used in the conventional full-field ERGs. A time constant of 0.03 seconds with a 100-Hz cutoff filter on the amplifier was used for recording the a- and b-waves, and a time constant of 0.003 seconds with a 300-Hz cutoff filter was used for recording the OPs.

The amplitude of the a-wave was measured from the baseline to the first negative trough, and the amplitude of the b-wave was measured from the trough of the a-wave to the positive peak of the b-wave. The amplitude of the OPs was calculated by summing the first three wavelets. The amplitudes of OPs were calculated for only the 10° and 15° stimulus spots, because the OPs elicited by the 5° spot were too small, even in normal eyes. The amplitude of the fmERG was considered to be nondetectable when it was less than the noise level (<0.4 μV).

The fmERGs elicited by this method have been shown to be generated by the cone system, and the responses elicited by spot stimuli of 5° to 15° have been shown to be local responses.[19,20]

Statistical Analyses

The significance of the differences between patients with RP and normal control subjects was analyzed using the nonparametric Mann-Whitney test. Differences in the amplitude or implicit times between 5° and 10° spots or between 10° and 15° spots were analyzed using the Wilcoxon signed rank test. Differences were considered to be significant at $P < 0.05$.

Results

Effect of Stimulus Spot Size

The fmERGs recorded from a normal subject and three representative patients with RP are shown in Figure 1. The a- and b-waves were recorded with a 0.03-second time constant (top trace) and the OPs by a 0.003-second time constant (bottom trace). Of the 39 patients with RP, only 2 had fmERG amplitudes within the normal range for all stimulus spot sizes (Fig. 1, Case 1). There were 37 patients whose fmERG amplitudes were detectable but smaller than the normal range for at least one stimulus size (Fig. 1; Case 2, Case 3).

The mean (±SD) of the amplitudes of the a-wave, b-wave, and OPs for the three stimulus spot sizes in the 39 patients with RP and 30 age-similar normal control subjects are shown in Table 1. The mean amplitudes of all ERG components were significantly smaller for all stimulus sizes in the patients with RP than in normal control subjects ($P < 0.0001$).

The amplitude of each component of the fmERGs in each patient was divided by the corresponding component of the normal control subject, and the relative data are plotted in Figure 2. We found that the degree of amplitude reduction became larger with increasing stimulus spot size for all components. The differences were statistically significant between 5° and 10° spots and between 10° and 15° spots for all components ($P < 0.05$, Fig. 2)

The mean (±SD) implicit times of all ERG components for all stimulus spots in our patients with RP and 30 age-similar normal control subjects are shown in Table 2. The data of some patients were not included in this table because it was difficult to measure their implicit time. The mean implicit times of all components in patients with RP were not significantly different from those in normal control subjects for the 5° and 10° spots, but were significantly delayed for the 15° spot except for OP3 (third positive wave of the OPs).

Waveform Changes of fmERGs in Patients with RP

We next studied the changes in the waveforms of fmERGs in our patients with RP. The amplitudes of all ERG components for the 39 patients with RP, expressed relative to the mean

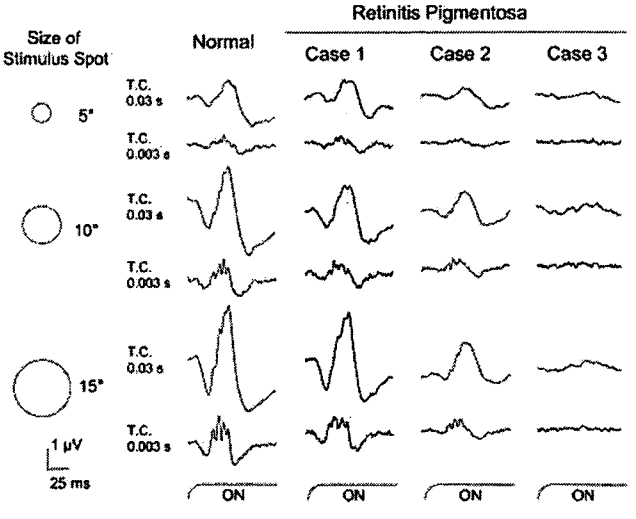

FIGURE 1. fmERGs recorded from one representative normal subject and three patients with RP. Two different time constants were used simultaneously for each recording. The a- and b-waves were recorded with a 0.03-second time constant (*top trace*) and the OPs with a 0.003-second time constant (*bottom trace*).

TABLE 1. Amplitude of Each ERG Component for Normal Control Subjects and Patients with RP

Spot Size	Waveform	Control	RP	*P*
5°	a-wave	0.59 ± 0.15	0.32 ± 0.18	<0.0001
	b-wave	1.53 ± 0.30	0.84 ± 0.38	<0.0001
10°	a-wave	1.40 ± 0.34	0.55 ± 0.28	<0.0001
	b-wave	3.52 ± 0.63	1.62 ± 0.62	<0.0001
	OPs	1.60 ± 0.43	1.08 ± 0.73	<0.0001
15°	a-wave	2.31 ± 0.56	0.83 ± 0.39	<0.0001
	b-wave	5.64 ± 0.98	2.29 ± 0.98	<0.0001
	OPs	3.17 ± 0.97	1.55 ± 1.03	<0.0001

Data are expressed as the mean ± SD. The Mann-Whitney test was used for statistical comparison.

TABLE 2. Implicit Time of Each ERG Component in Normal Control Subjects and Patients with RP

Spot Size	Waveform	Control	RP (*n*)	*P*
5°	a-wave	20.9 ± 2.6	21.6 ± 4.4 (38)	0.54
	b-wave	44.7 ± 2.9	45.2 ± 3.4 (38)	0.34
10°	a-wave	19.5 ± 1.9	21.0 ± 2.7 (39)	0.05
	b-wave	42.6 ± 3.3	44.0 ± 3.0 (39)	0.06
	OP1	24.1 ± 2.0	24.9 ± 1.9 (34)	0.09
	OP2	30.6 ± 2.1	31.6 ± 2.8 (34)	0.21
	OP3	36.8 ± 2.0	37.9 ± 3.0 (30)	0.26
15°	a-wave	19.4 ± 1.6	20.6 ± 2.7 (39)	0.02
	b-wave	40.7 ± 3.1	43.7 ± 3.0 (39)	<0.0001
	OP1	23.5 ± 1.7	24.6 ± 1.6 (36)	0.02
	OP2	30.0 ± 2.0	31.2 ± 2.3 (36)	0.04
	OP3	36.5 ± 2.2	37.2 ± 2.2 (34)	0.38

Data are expressed as the mean ± SD. The Mann-Whitney test was used for statistical comparison.

amplitudes in normal control subjects, are plotted in Figure 3. In patients with RP, the amplitudes of the OPs were better preserved than those of the b-waves for the 10° spot, and the b-waves were better preserved than the a-waves (Fig. 3A). The mean relative amplitude was 0.67 for the OPs, 0.46 for the b-wave, and 0.39 for the a-wave. The differences in the relative amplitude between these three components were statistically significant for the 10° spot ($P < 0.05$). A similar tendency was also seen for 15° spot, but the difference between the OPs and the b-wave was not significant ($P = 0.15$, Fig. 3B).

Next, we plotted the individual amplitudes of the different components of the fmERGs from the patients with RP. In Figure 4A, the amplitudes of the b-wave are plotted against the amplitudes of the a-wave elicited by the 10° spot in all 39 patients with RP and 30 normal control subjects. The shaded area shows the range of normal controls, and the dotted lines show the mean amplitudes in the normal control subjects. We found that the majority of the patients with RP (27, 69.2%) had fmERGs with amplitudes that were lower than the lowest limit of normal range for both the a- and b-waves.

The amplitudes of the OPs elicited by the 10° stimulus spot are plotted against the amplitude of the b-wave for all 39 patients with RP and 30 normal control subjects in Figure 4B. As in Figure 4A, the shaded area shows the range in the normal control subjects, and the dotted line shows the mean amplitudes in the normal control subjects.

Ten (25.6%) patients with RP had normal OP amplitudes with reduced b-wave amplitude, whereas none of the patients had normal b-wave amplitude with reduced OP amplitudes. These results combined with the data of Figure 3 indicate that the amplitudes of the OPs were better preserved than those of the b-wave for a 10° spot size in the patients with RP. We also noticed that the amplitude of OPs was larger than the upper limit of the normal range in one RP patient (Fig. 4B, arrowhead).

The fmERGs of three representative patients with RP who had a larger than normal OP/b-wave ratio are shown in Figure 5. It is clear that in these patients, the OPs were better preserved than were the a- and b-waves.

DISCUSSION

Our results showed that the degree of amplitude reduction and delay of implicit time became greater with increasing stimulus size (Tables 1, 2, Fig. 2). These results are not surprising when one considers the typical pattern of retinal dysfunction in RP. In most patients with RP, the retina is progressively impaired from the periphery to the central area. Past electrophysiological results of studies in which fERGs or mfERGs were used[5,6,10–17] are in accord with our results.

Although fERGs and mfERGs have been extensively investigated in patients with RP,[5–17] there are only a few studies in which different ERG components that originate from different retinal layers were investigated. Falsini et al.[9] analyzed the fundamental and second harmonic components of fmERGs, which are believed to originate from outer and inner retinas,

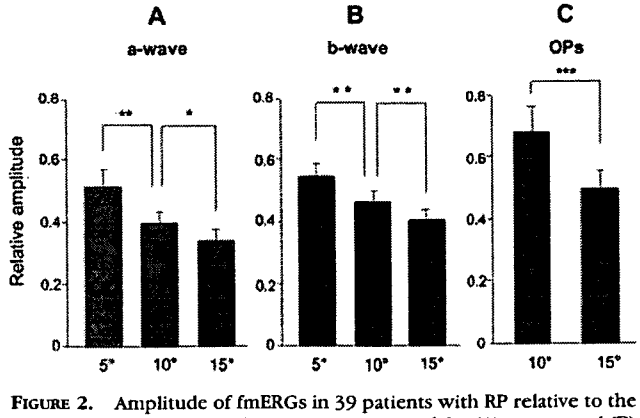

FIGURE 2. Amplitude of fmERGs in 39 patients with RP relative to the mean in normal control subjects. Comparison of the (A) a-wave and (B) b-wave amplitudes for 5°, 10°, and 15° spots. (C) Comparison of the OP amplitude for 10° and 15° spot. Bar, SEM. $^{*}P < 0.05$, $^{**}P < 0.01$, $^{***}P < 0.001$.

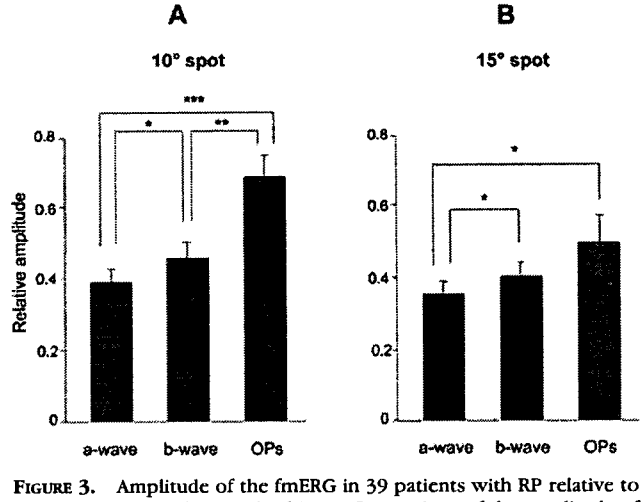

FIGURE 3. Amplitude of the fmERG in 39 patients with RP relative to the mean in normal control subjects. Comparison of the amplitude of each component for the (A) 10° and (B) 15° spot. Bar, SEM. $^{*}P < 0.05$, $^{**}P < 0.01$, $^{***}P < 0.001$.

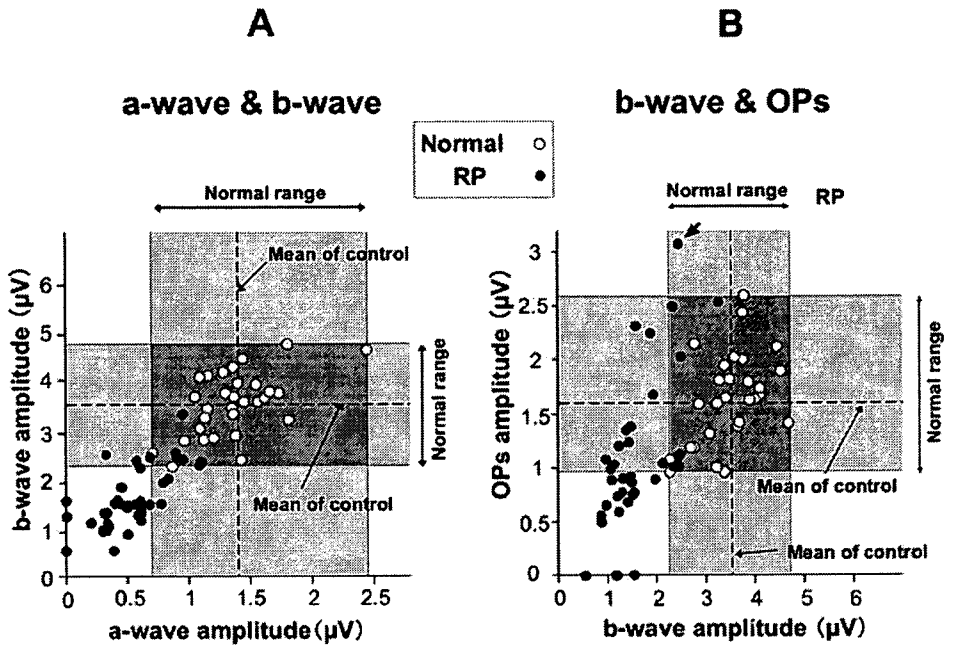

FIGURE 4. Plot of the b-wave amplitude against the amplitude of the a-wave (A), and amplitude of the OPs against the amplitude of the b-wave (B) in 30 normal subjects and 39 patients with RP. Results for the 10° stimulus spot are shown. *Shaded area*: the range of normal subjects; *dotted line*: mean of normal subjects.

respectively. They found that the ratio of the amplitudes of the fundamental component to the second harmonic component was larger in the RP group than that of normal control subjects. From these results, they concluded that not only the outer retina but also the inner retina contributed to the macular dysfunction in eyes with RP. Other ERG studies using full-field stimuli also demonstrated that neural cells postsynaptic to the photoreceptors contributed to the retinal dysfunction in eyes with RP.[21,22]

A new, interesting finding in this study was that the amplitudes of the OPs were better preserved than those of the a- and b-waves for a 10° spot in our patients with early-stage RP. The relative amplitude of the mean value in normal control subjects for the 10° spot was 0.67 for the OPs, and this value was significantly larger than that for the b-wave (0.46), which in turn was larger than that of the a-wave (0.39; Fig. 3A). In addition, 26% of the patients with RP had normal OP amplitudes with reduced b-wave amplitude, whereas none of the patients had normal b-wave amplitude with reduced OPs amplitudes (Fig. 4B).

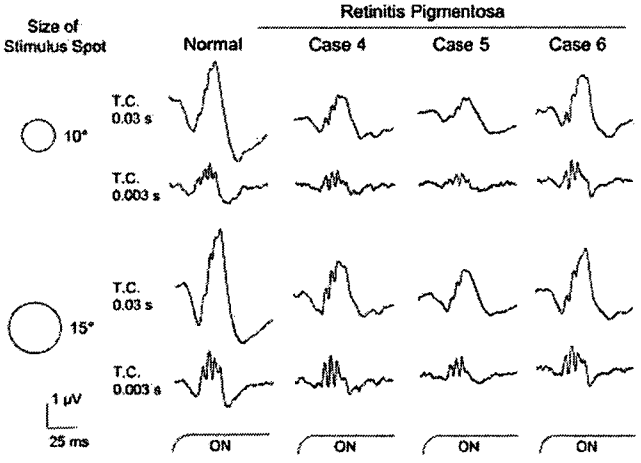

FIGURE 5. fmERGs from three patients with RP whose amplitude ratios of the OPs to the b-wave (OPs/b) are larger than the normal range for both 10° and 15° stimulus spots. Two different time constants were used simultaneously for each recording. The a- and b-waves were recorded with a 0.03-second time constant (*top*) and the OPs with a 0.003-second time constant (*bottom*). Note that the OP amplitude of Case 6 for the 10° spot is larger than the upper limit of normal control subjects (see also Fig. 4B, *arrowhead*).

Although the retinal origin of each component of fmERG has not been completely determined, one can assume their origins based on recent experiments in primates. The initial photopic a-wave is thought to originate mainly from cone photoreceptors and the cone off-bipolar cells.[23,24] The photopic b-wave is determined by the combined activities of the cone on- and off-bipolar cells.[25–27] The origins of the OPs are thought to be from feedback neural pathways in the inner part of the retina, especially around the inner plexiform layer, including the amacrine cells and partly the ganglion cells.[28–30] Recent studies[28–30] have suggested that the origins of OPs are dependent not only on individual wavelets, but also on response frequencies. Thus, our results strongly suggest that in our patients at a relatively early stage of RP, the retinal activities from the inner retinal layer (OPs) were better preserved than those from the middle and outer layers (the b- and a-waves).

The exact mechanism for the relative preservation of the macular OPs in early-stage patients with RP was not investigated in this study. We have studied the effect of stimulus intensity on the amplitude of each component of the fmERG and have found that with decreasing stimulus intensities, the a-wave, b-wave, and OPs decreased proportionally.[31] These results suggest that the waveform changes of fmERGs seen in our patients with RP cannot be explained simply by a decrease in the sensitivity to light.

The preservation of macular OPs in patients with RP is quite interesting when considering the spatial distribution of macular OPs in normal subjects. We have studied the spatial distribution of OPs in the macular area for normal subjects using an annulus (center off) stimulus to elicit fmERGs and have found that in normal subjects, the amplitude of the OPs was greater in the parafovea and perifovea. Therefore, we initially expected that the amplitudes of OPs would be more reduced

than those of the a- and b-waves for 10° and 15° spots in patients with RP, because the parafovea and perifovea was thought to be more damaged than the fovea in patients with RP. However, our results were just the opposite: The amplitudes of the OPs tended to be more preserved than those of the a- and b-waves for 10° and 15° spots in patients with RP (Fig. 3). Thus, it is interesting to consider why some patients with RP show such a selective preservation of OPs.

We have two hypotheses for the mechanism that preserves the macular OPs in patients with RP. First is the buffering effect of the large receptive fields of the OP generators, viz., the amacrine cells and ganglion cells. Histopathological studies have shown that a large percentage of the inner retinal neurons remain histologically intact even though most photoreceptors were lost in patients with RP.[32-34] Sufficient electrical activity from the inner retina may be produced by the large receptive fields, even though the electrical activities from outer and middle retinal layers are decreased as a consequence of progression of the RP. However, it is difficult to explain all the present results only by this mechanism. For example, why did one of our patients with RP (Fig. 4B, arrowhead) have supernormal OPs, despite lower borderline amplitude of the b-wave?

The second hypothesis is that the preservation of OPs in patients with RP may be due to retinal remodeling after the progressive loss of photoreceptors, to compensate for decreasing signal input to middle and inner retina. Evidence has been accumulating to support this idea in animal models of retinal degeneration.[34-40] Alman et al.[36] demonstrated that there is a compensatory synaptogenesis in reaction to partial loss of photoreceptors in rats with a rhodopsin mutation. Jones et al.[39] have shown that after loss of the outer nuclear layer, various kinds of retinal remodeling were observed not only in rodent models of photoreceptor degeneration but also in humans with RP. Our results may be a clinical demonstration that such compensatory changes can occur in some patients at the early stage of RP. However, such compensatory retinal remodeling may not occur in all patients with RP, because there was a large variation in the ratio of OPs/b-wave in our patients with RP (Fig. 4B). Such variations may be due to the different stages and severities of the disease, different genetic backgrounds, or different environmental effects.

There are some limitations to our study. First, the study was performed retrospectively, and the selection of patients was not performed randomly. Second, we did not perform molecular testing on our patients with RP and could not characterize the pattern of fmERG as a consequence of specific gene mutation. Third, we did not compare the findings of the fmERGs with detailed psychophysical results (e.g., rod and cone perimetry) or macular morphologic tests (e.g., optical coherence tomography). Further studies are needed to clarify the mechanism of the fmERGs waveform changes in patients with RP.

In conclusion, our results demonstrated that electrical activities from the inner retina are preserved better than those from middle and inner retinal layers in the central retina of patients with early-stage RP. These results can provide important information on the pathophysiology of and possible future treatment for RP.

References

1. Carr RE, Heckenlively JR. Hereditary pigmentary degenerations of the retina. In: Duane TD, Jaeger EA, eds. *Clinical Ophthalmology*. Philadelphia: JB Lippincott; 1987:1-28.
2. Heckenlively JR. RP syndromes. In: Heckenlively JR, ed. *Retinitis Pigmentosa*. Philadelphia: JB Lippincott; 1988:221-252.
3. Newsome DA. Retinitis pigmentosa, Usher's syndrome, and other pigmentary retinopathies. In: Newsome DA, ed. *Retinal Dystrophies and Degenerations*. New York: Raven Press; 1988:161-194.
4. Weleber RG, Gregory-Evance K. Retinitis pigmentosa and allied disorders. In: Hinton DR, ed. *Basic Science and Inherited Retinal Disease*. 4th ed. St. Louis: Mosby; 2006:395-498. *Retina*; vol. 1.
5. Sandberg MA, Effron MH, Berson EL. Focal cone electroretinograms in dominant retinitis pigmentosa with reduced penetrance. *Invest Ophthalmol Vis Sci*. 1978;17:1096-1101.
6. Sandberg MA, Jacobson SG, Berson EL. Foveal cone electroretinograms in retinitis pigmentosa and juvenile macular degeneration. *Am J Ophthalmol*. 1979;88:702-707.
7. Biersdorf WR. Temporal factors in the foveal ERG. *Curr Eye Res*. 1982;1:717-722.
8. Seiple W, Siegel IM, Carr RE, Mayron C. Evaluating macular function using the focal ERG. *Invest Ophthalmol Vis Sci*. 1986;27:1123-1130.
9. Falsini B, Iarossi G, Porciatti V, et al. Postreceptoral contribution to macular dysfunction in retinitis pigmentosa. *Invest Ophthalmol Vis Sci*. 1994;35:4282-4290.
10. Hood DC, Holopigian K, Greenstein V, Seiple W, Li J, Sutter EE, Carr RE. Assessment of local retinal function in patients with retinitis pigmentosa using the multi-focal ERG technique. *Vision Res*. 1998;38:163-179.
11. Chan HL, Brown B. Investigation of retinitis pigmentosa using the multifocal electroretinogram. *Ophthalmic Physiol Opt*. 1998;18:335-350.
12. Seeliger MW, Kretschmann UH, Apfelstedt-Sylla E, Zrenner E. Implicit time topography of multifocal electroretinograms. *Invest Ophthalmol Vis Sci*. 1998;39:718-723.
13. Felius J, Swanson WH. Photopic temporal processing in retinitis pigmentosa. *Invest Ophthalmol Vis Sci*. 1999;40:2932-2944.
14. Hood DC. Assessing retinal function with the multifocal technique. *Prog Retin Eye Res*. 2000;19:607-646.
15. Holopigian K, Seiple W, Greenstein VC, Hood DC, Carr RE. Local cone and rod system function in patients with retinitis pigmentosa. *Invest Ophthalmol Vis Sci*. 2001;42:779-788.
16. Vajaranant TS, Seiple W, Szlyk JP, Fishman GA. Detection using the multifocal electroretinogram of mosaic retinal dysfunction in carriers of X-linked retinitis pigmentosa. *Ophthalmology*. 2002;109:560-568.
17. Robson AG, Saihan Z, Jenkins SA, et al. Functional characterisation and serial imaging of abnormal fundus autofluorescence in patients with retinitis pigmentosa and normal visual acuity. *Br J Ophthalmol*. 2006;90:472-479.
18. Marmor MF, Holder GE, Seeliger MW, Yamamoto S. International Society for Clinical Electrophysiology of Vision. Standard for clinical electroretinography (2004 update). *Doc Ophthalmol*. 2004;108:107-114.
19. Miyake Y, Shiroyama N, Ota I, Horiguchi M. Oscillatory potentials in electroretinograms of the human macular region. *Invest Ophthalmol Vis Sci*. 1988;29:1631-1635.
20. Miyake Y. Studies of local macular ERG (in Japanese). *Acta Soc Ophthalmol Jpn*. 1988;92:1418-1449.
21. Cideciyan AV, Jacobson SG. Negative electroretinograms in retinitis pigmentosa. *Invest Ophthalmol Vis Sci*. 1993;34:3253-3263.
22. Hood DC, Birch DG. Abnormalities of the retinal cone system in retinitis pigmentosa. *Vision Res*. 1996;36:1699-1709.
23. Bush RA, Sieving PA. A proximal retinal component in the primate photopic ERG a-wave. *Invest Ophthalmol Vis Sci*. 1994;35:635-645.
24. Robson JG, Saszik SM, Ahmed J, Frishman LJ. Rod and cone contributions to the a-wave of the electroretinogram of the macaque. *J Physiol*. 2003;547:509-530.
25. Knapp AG, Schiller PH. The contribution of on-bipolar cells to the electroretinogram of rabbits and monkeys: a study using 2-amino-4-phosphonobutyrate (APB). *Vision Res*. 1984;24:1841-1846.
26. Sieving PA, Murayama K, Naarendorp F. Push-pull model of the primate photopic electroretinogram: a role for hyperpolarizing neurons in shaping the b-wave. *Vis Neurosci*. 1994;11:519-532.
27. Rangaswamy NV, Hood DC, Frishman LJ. Regional variations in local contributions to the primate photopic flash ERG: revealed

using the slow-sequence mfERG. *Invest Ophthalmol Vis Sci.* 2003; 44:3233-3247.

28. Heynen H, Wachtmeister L, van Norren D. Origin of the oscillatory potentials in the primate retina. *Vision Res.* 1985;25:1365-1373.
29. Wachtmeister L. Oscillatory potentials in the retina: what do they reveal. *Prog Retin Eye Res.* 1998;17:485-521.
30. Rangaswamy NV, Zhou W, Harwerth RS, Frishman LJ. Effect of experimental glaucoma in primates on oscillatory potentials of the slow-sequence mfERG. *Invest Ophthalmol Vis Sci.* 2006;47:753-767.
31. Shiroyama N, Miyake Y. Analysis of focal macular ERG in idiopathic central serous chorioretinopathy (in Japanese). *Nippon Ganka Gakkai Zasshi.* 1990;94:1048-1056.
32. Stone JL, Barlow WE, Humayun MS, de Juan E Jr, Milam AH. Morphometric analysis of macular photoreceptors and ganglion cells in retinas with retinitis pigmentosa. *Arch Ophthalmol.* 1992; 110:1634-1639.
33. Santos A, Humayun MS, de Juan E Jr, et al. Preservation of the inner retina in retinitis pigmentosa: a morphometric analysis. *Arch Ophthalmol.* 1997;115:511-515.
34. Milam AH, Li ZY, Fariss RN. Histopathology of the human retina in retinitis pigmentosa. *Prog Retin Eye Res.* 1998;175-205.
35. Machida S, Kondo M, Jamison JA, et al. P23H rhodopsin transgenic rat: correlation of retinal function with histopathology. *Invest Ophthalmol Vis Sci.* 2000;41:3200-3209.
36. Aleman TS, LaVail MM, Montemayor R, et al. Augmented rod bipolar cell function in partial receptor loss: an ERG study in P23H rhodopsin transgenic and aging normal rats. *Vision Res.* 2001;41: 2779-2797.
37. Banin E, Cideciyan AV, Aleman TS, et al. Retinal rod photoreceptor-specific gene mutation perturbs cone pathway development. *Neuron.* 1999;23:549-557.
38. Peng YW, Hao Y, Petters RM, Wong F. Ectopic synaptogenesis in the mammalian retina caused by rod photoreceptor-specific mutations. *Nat Neurosci.* 2000;3:1121-1127.
39. Jones BW, Watt CB, Frederick JM, et al. Retinal remodeling triggered by photoreceptor degenerations. *J Comp Neurol.* 2003;464: 1-16.
40. Marc RE, Jones BW, Watt CB, Strettoi E. Neural remodeling in retinal degeneration. *Prog Retin Eye Res.* 2003;22:607-655.

Available online at www.sciencedirect.com
ScienceDirect
Vision Research 48 (2008) 273–280
Vision Research
www.elsevier.com/locate/visres

Comparison of focal macular cone ERGs in complete-type congenital stationary night blindness and APB-treated monkeys ☆

Mineo Kondo *, Shinji Ueno, Chang-Hua Piao, Yozo Miyake, Hiroko Terasaki

Department of Ophthalmology, Nagoya University Graduate School of Medicine, 65 Tsuruma-cho, Showa-ku, Nagoya 466-8550, Japan

Received 1 August 2007; received in revised form 9 November 2007

Abstract

Focal macular cone electroretinograms (ERGs) and multifocal ERGs were recorded to study the macular function in patients with the complete-type of congenital stationary night blindness (cCSNB). The waveforms of the focal macular cone ERGs and the on- and off-responses of the multifocal ERGs in the cCSNB patients were similar to those recorded from monkey retinas treated with L-2 amino-4-phosphonobutyric acid (APB), suggesting that patients with cCSNB have a complete defect of the on-pathway even in the central retina. The results also demonstrated that there was a paradoxical positive response in the central retina of cCSNB patients, as compared to the negative full-field ERGs in the same subjects.

Keywords: Electroretinogram (ERG); Focal macular cone ERG; Congenital stationary night blindness (CSNB); Complete-type; APB (L-2 amino-4-phosphonobutyric acid)

1. Introduction

The complete-type of congenital stationary night blindness (cCSNB) is a non-progressive retinal disease characterized by congenital night blindness with a moderate decrease of the visual acuity and myopia (Miyake, Horiguchi, Suzuki, Kondo, & Tanikawa, 1997; Miyake, Yagasaki, Horiguchi, Kawase, & Kanda, 1986). The inheritance pattern of cCSNB is usually X-linked or autosomal recessive. It was recently reported that most X-linked cCSNB resulted from mutations in the *NYX* gene (Bech-Hansen et al., 2000; Pusch et al., 2000), and some cases of autosomal recessive cCSNB resulted from mutations in the *MGR6* gene (Dryja et al., 2005).

cCSNB patients have very characteristic electroretinograms (ERGs). When elicited by a bright stimulus after dark-adaptation, the ERGs are the negative-type with an a-wave of normal amplitude and a b-wave that is smaller than the a-wave. When a long-duration photopic stimulus is used, the b-waves of the ERGs of cCSNB patients are severely reduced while the off-response d-wave is well-preserved (Houchin, Purple, & Wirtschafter, 1991; Miyake, Yagasaki, Horiguchi, & Kawase, 1987; Young, 1991). These ERG waveforms are very similar to those in the monkey photopic ERGs after an intravitreal injection of 2-amino-4-phosphonobutyric acid (APB), which blocks neurotransmission from photoreceptors to the on-bipolar cells (Evers & Gouras, 1986; Knapp & Schiller, 1984; Sieving, Murayama, & Naarendorp, 1994). These results demonstrated that the defect in the neural pathway of cCSNB patients lies in the signal transmission from the photoreceptors to the depolarizing on-bipolar cells (DBCs) in both the rod and cone pathways. Recent ERG analysis using sinusoidal and ramping on/off flicker stimuli also indicated that the deficit in eyes with cCSNB is localized to the DBC pathway with no apparent involvement of the hyperpolarizing off-bipolar cells (HBCs) (Khan et al., 2005).

☆ *Grant support:* Grant-in Aid 14770952 (M.K.), and 14370557 (H.T.) from the Ministry of Education, Science, Sports and Culture, Japan.
* Corresponding author. Fax: +81 52 744 2278.
E-mail address: kondomi@med.nagoya-u.ac.jp (M. Kondo).

0042-6989/$ - see front matter © 2007 Elsevier Ltd. All rights reserved.
doi:10.1016/j.visres.2007.11.010

Although there are many electrophysiological studies on the full-field ERG in patients with cCSNB, there are very few studies on the macular function of eyes with cCSNB using either the multifocal or focal macular cone ERG techniques (Kondo et al., 2001; Leifert, Todorova, Prunte, & Palmowski-Wolfe, 2005). During our extensive studies of the complete and incomplete type of CSNB, we have been gaining the impression that the cone on-pathway may be functioning relatively well only in the central retina in cCSNB because these patients have relatively good visual function in the central field (Miyake et al., 1997; Terasaki et al., 1999).

The purpose of this study was to investigate the macular function of patients with cCSNB in more detail using focal macular cone ERGs and multifocal ERGs. To accomplish this, we separated the on- and off-responses of the photopic ERGs using long-duration photopic stimuli in the macular area of patients with cCSNB, and then compared the obtained waveforms with those recorded from monkey retinas in which the on-pathway was completely blocked pharmacologically by an intravitreal injection of L-2 amino-4-phosphonobutyric acid (APB).

2. Materials and methods

2.1. Patients with complete-type CSNB

From the patients with cCSNB examined in our clinic (Department of Ophthalmology, Nagoya University Hospital), we selected three patients who agreed to participate and were cooperative with the electrophysiological examinations (Table 1). All patients had poor night vision from birth and had no fundus abnormalities except for myopic changes. Their corrected visual acuities were 0.4, 0.4, and 0.6, and the rod branch of the dark-adaptation curve was missing as determined by psychophysical dark adaptometry. The full-field ERG rod responses were undetectable, and the rod and cone mixed maximal ERG had a negative-shape with no detectable oscillatory potentials.

An informed consent was obtained from the three patients after a full explanation of the procedures. All studies were conducted in accordance with the principles embodied in the Declaration of Helsinki.

2.2. Animals

Four rhesus (*Macaca mulata*) monkeys were studied under protocols approved by Nagoya University School of Medicine. All experiments were conducted in accordance with NIH guidelines on animal use and with the ARVO statement on the Use of Animals in Ophthalmic and Vision Research. The animals were anesthetized with intramuscular injection of ketamine hydrochloride (7 mg/kg, 5–10 mg/kg/h maintenance dose) and xylazine (0.6 mg/kg). The respiration and heart rate were monitored, and hydration was maintained by a slow, continuous infusion of lactated Ringer solution. The cornea was anesthetized by topical 1% tetracaine, and the pupil was dilated with topical 0.5% tropicamide, 0.5% phenylephrine HCL, and 1% atropine.

2.3. Drug application to animals

The drugs were injected into the vitreous with a 30-gauge needle inserted through the pars plana approximately 3 mm posterior to the limbus. The drugs (Sigma Chemical Co., St. Louis, MO) were dissolved in sterile saline and injected in amounts of 0.05–0.07 ml. The intravitreal concentration was 1–2 mM for L-2 amino-4-phosphonobutyric acid (APB) and 5 mM for *cis*-2, 3 piperidine dicarboxylic acid (PDA). Recordings were begun about 60–90 min after the drug injections, and studies were completed within 5 h. Although the drug effects are mostly reversible after a recovery period of several weeks, the results that are presented were recorded from the eyes not previously treated.

2.4. Focal macular cone ERG

Focal macular cone ERGs were elicited by stimulating the macula with small stimulus spots (Miyake, 1988b; Miyake, Shiroyama, Ota, & Horiguchi, 1988a). The position of the spot on the fundus was monitored during the recording with a modified infrared fundus camera. The Burian-Allen bipolar contact lens electrode (Hansen Ophthalmic Development Laboratories, Iowa City, IA) which was used to record the focal macular cone ERGs, allowed a clear view of the fundus on the television monitor. The luminances of the stimulus and the background were 30.0 cd/m^2 and 3.0 cd/m^2, respectively. A 5-Hz rectangular stimulus (100 ms-on and 100 ms-off) was used with a stimulus spot of 15 degrees in diameter. A total of 512 responses were averaged by a signal processor, and the time constant was 0.03 s with a 300-Hz high-cut filter. The ERG responses produced by this method are generated by the cone system, and the responses elicited by the spot stimuli are considered to be local responses (Miyake, 1988b; Miyake et al., 1988a).

2.5. Recording multifocal on- and off-responses

Our method for recording on- and off-responses of the multifocal ERGs has been described in detail (Kondo & Miyake, 2000; Kondo, Miyake, Horiguchi, Suzuki, & Tanikawa, 1998). In brief, multifocal ERGs were obtained with the VERIS system (EDI, San Mateo, CA). The stimulus array consisted of 61 hexagonal elements that were displayed on a CRT monitor (GDM, Sony, Tokyo, Japan) and driven at 75 frames/s. At a viewing distance of 27 cm, the subtense of the visual field was approximately 50°.

To obtain on- and off-responses with the VERIS system, we used consecutive white TV frames. Each hexagon was modulated between two stimulus patterns according to a binary m-sequence: eight consecutive white frames followed by eight consecutive dark frames (pattern A) or 16 consecutive dark frames (pattern B). In this stimulus setting, a stimulus is not continuously bright during its bright phase because the focal flash decays within a few milliseconds. However, there is evidence that a high-frequency train of flashes can roughly simulate the effects produced by a long-duration stimulus and thus can produce a corneal positive off-response (Saeki & Gouras, 1996; Young, 1991).

Based on our preliminary study, the following stimulus parameters were found to be suitable for eliciting maximal on- and off-responses from each local retinal area: stimulus intensity of 120 cd/m^2 with a duration of 8 frames (106 ms) on a 20 cd/m^2 background illumination. The m-sequence stimulation rate was, therefore, 4.7/s and the base interval was 213.3 ms (Kondo & Miyake, 2000; Kondo et al., 1998).

Table 1
Clinical characteristics of three patients with complete type CSNB

Case	Age	Sex	Inheritance pattern	Refractive error (*D*)	Visual acuity
Case 1	54	M	Autosomal recessive	−4.0	0.4
Case 2	20	M	X-linked	−9.5	0.4
Case 3	15	F	Autosomal recessive	−6.0	0.6

The signals were amplified by 100 K and filtered between 3 and 300 Hz (Grass, Quincy, MA). The data sampling rate was 1200 Hz. To reduce the artifacts due to eye movements, an "artifact rejection" algorithm (VERIS software, EDI) was used once (Marmor et al., 2003). The length of the m-sequence used was 2^{11}–1. Thus, the total recording took 7.3 min, and it was divided into 16 segments.

For recording multifocal ERGs from monkeys, a modified ophthalmoloscopic technique was used to locate the projection of the fovea on the center of the stimulus pattern (Rangaswamy, Hood, & Frishman, 2003). This modified ophthalmoscope was kindly provided by Dr. L. Frishman (University of Houston). The position of the fovea was checked frequently before and after the multifocal ERG recordings.

2.6. Recording full-field ERGs

Full-field ERGs were recorded with long-duration stimuli (166 ms or 100 ms) using a densely-packed array of 102 green LEDs (525 nm peak wavelength; 50 nm at half-amplitude). The array was positioned at the top of the Ganzfeld dome and covered by a diffuser (Ueno et al., 2006). The LEDs were controlled by a digital function generator (WF1945, NF Corporation, Tokyo, Japan). The stimulus intensity and background illumination measured in the dome was 120 cd/m^2 and 40 cd/m^2, respectively. In the last experiment, the stimulus intensity and background illumination was set at 30 cd/m^2 and 3 cd/m^2, respectively, in order to compare the waveforms of full-field ERG and focal macular cone ERG at the same stimulus and background condition.

After 10 min of light adaptation, ERGs were recorded with a Burian-Allen bipolar contact lens electrode (Hansen Ophthalmic Development Labs, Iowa City, IA). A ground electrode was attached to the ipsilateral ear. Responses were amplified by 10 K and the bandpass was set to 0.3–1000 Hz. The data were digitized at 4.3 kHz. Twenty responses were averaged (Power Lab, AD Instruments, Castle Hill, Australia).

3. Results

3.1. Focal macular cone ERGs in cCSNB

Representative focal macular cone ERGs recorded from a myopic control (38-year-old man; refractive error, −5.50 D) and the three patients with cCSNB are shown in the left panel of Fig. 1. The waveforms from the three patients are clearly different from those of the myopic control: the amplitudes of the a-waves are normal, but the amplitudes of the following positive wave are smaller than the b-wave of the myopic control (see also Table 2). These changes resulted in a reduced b-wave to a-wave (b/a) ratio. In addition, the implicit times of the a- and b-waves in

Table 2
Amplitudes and implicit times of focal macular ERGs (FMERGs) from three patients with complete type CSNB and 15 patients with myopic controls

	Amplitude (μV)			Implicit times (ms)	
	a-wave	b-wave	b/a ratio	a-wave	b-wave
Case 1	2.4	2.4	1.0	21.4	47.2
Case 2	1.9	2.9	1.56	28.0	46.8
Case 3	2.4	3.1	1.29	28.0	59.5
Myopic controls ($n = 15$)	2.0 ± 0.5	5.1 ± 0.9	2.51 ± 0.44	19.6 ± 1.7	40.9 ± 3.0

Data in myopic controls are expressed as the mean ± SD.

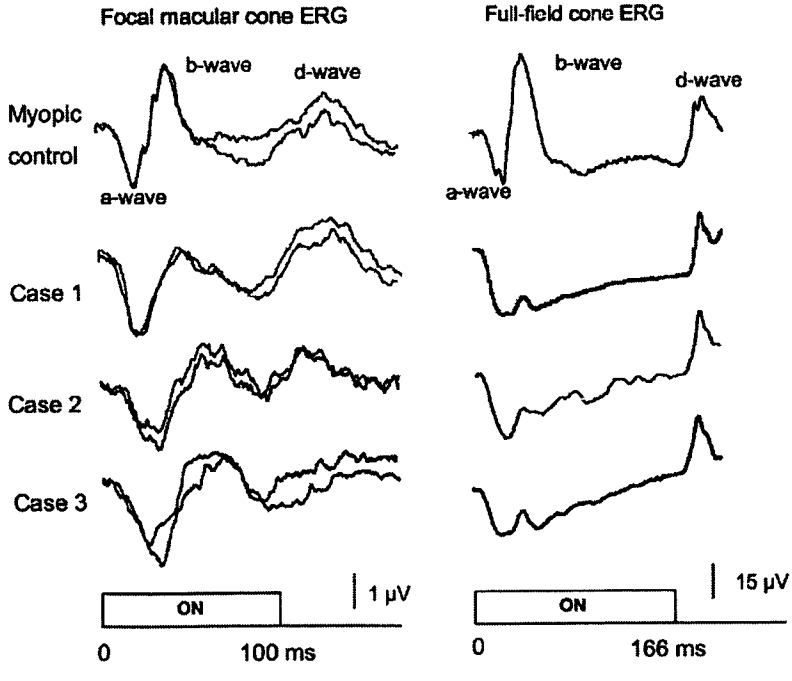

Fig. 1. Focal macular cone ERGs (left panel) and full-field ERGs (right panel) elicited by long duration stimuli recorded from a myopic control and three patients with complete-type congenital stational night blindness (cCSNB). Note that the amplitude ratios of the positive wave to the a-wave was <1.0 for the full-field ERG, but >1.0 for focal macular cone ERGs in the cCSNB patients.

cCSNB patients were prolonged (Table 2). The d-waves seen at the offset of the stimulus was not so prominent for both myopic controls and patients.

The full-field, photopic ERGs elicited by a long-duration stimulus (166 ms) from the same subjects are shown in the right panel of Fig. 1. In all three cCSNB patients, the b/a amplitude ratio was clearly <1.0 resulting in a "negative" ERG waveform.

3.2. Focal macular cone ERGs in monkey retina after APB

It is known that the on-response b-wave of the photopic long-flash ERG originates mainly from the neural activity of the cone depolarizing bipolar cells (DBCs) (Knapp & Schiller, 1984; Sieving et al., 1994). Based on the focal macular cone ERGs in the cCSNB patients, we thought that the function of cone on-pathway may be preserved to some degrees in the central retina of the cCSNB patients. To test this hypothesis, it was necessary to record the focal macular cone ERGs from the monkey retina after the cone on-pathway was completely blocked pharmacologically by APB, and to compare these waveforms with those from cCSNB patients.

The focal macular cone ERGs recorded from two rhesus monkeys before and after intravitreous injection of APB are shown in Fig. 2. After the APB injection, the a-wave amplitude became larger, and the peak time of the a- and the following positive wave became prolonged. The d-wave was slightly enhanced after APB. The ratio of the b-wave to the a-wave amplitudes became smaller than controls, but was still larger than 1.0 (monkey #1, 1.24; monkey #2, 1.33).

We initially interpreted this to indicate that remaining positive wave might be caused by an incomplete blockage of APB and thus injected more APB. However, the addition of APB did not change the waveforms of the focal macular cone ERGs, and the b/a amplitude ratio still remained greater than 1.0 even after increasing the APB concentration to twice the original concentration (2 mM).

The similarity in the waveforms between cCSNB patients and monkeys treated with APB indicated that the cone on-pathway seemed be completely blocked even in the central retina in cCSNB.

3.3. Multifocal on- and off-responses in cCSNB and APB-treated monkey

We also noted that the waveforms of photopic ERG with long duration stimuli were different between full-field cone ERGs and focal macular cone ERGs in cCSNB patients; the amplitude of remaining positive wave was still larger than that of the a-wave, whereas the amplitude ratio of the positive wave to the a-wave was always less than 1.0 for the full-field ERGs (Fig. 1). However, these differences in the waveform could be due to the different stimulus and recording conditions in the two methods. Therefore, we next compared these waveforms between the central and peripheral retinas directly in a patient with cCSNB. For

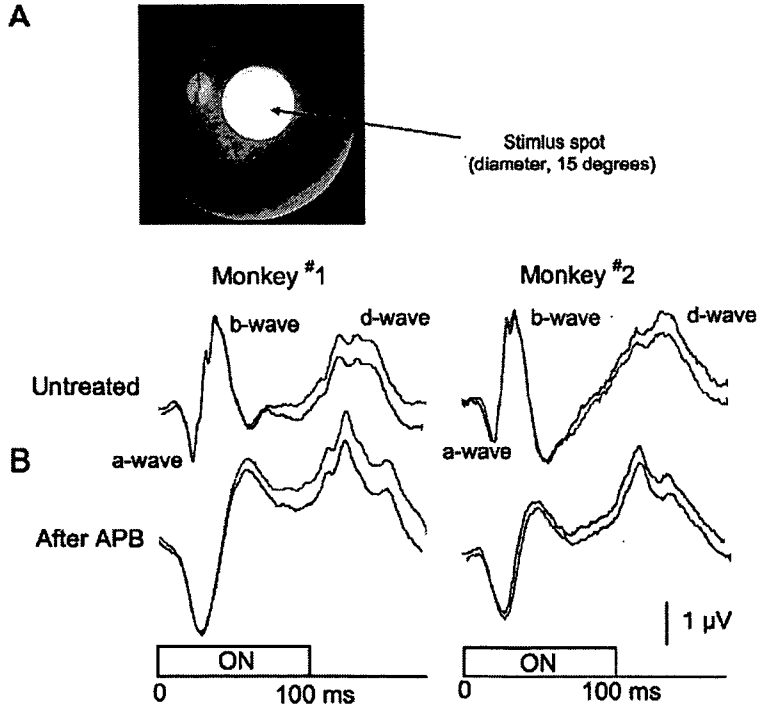

Fig. 2. Stimulus location and focal macular cone ERGs recorded from two monkeys. (A) Fundus photographs showing the stimulus spot. The 15° stimulus spot (diameter) was focused on the fovea. (B) Waveforms of focal macular cone ERGs before and after intravitreal injection of APB for two rhesus monkeys. Intravitreous concentration of APB was 1.0 mM.

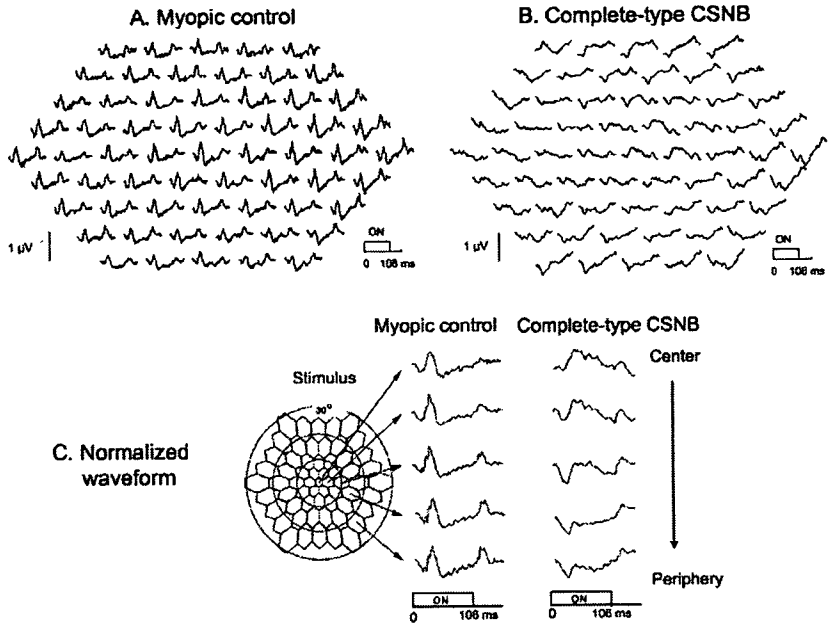

Fig. 3. Multifocal on- and off- responses using eight consequtive white frames. (A) Results from a myopic control. (B) Results from a patient with cCSNB (Case 1). (C) Normalized waveforms from five eccentric rings. Note that in cCSNB, the amplitude ratio of the positive wave to the a-wave is >1.0 in the central retina, but gradually become smaller towards to the periphery.

this purpose, we recorded the multifocal on- and off-responses (Kondo & Miyake, 2000; Kondo et al., 1998).

The multifocal on- and off-responses recorded from a representative myopic control (A), and a patient with cCSNB (B, Case 1 of Table 1) are shown in Fig. 3. It was clear that when compared to myopic control, the amplitudes of the positive wave are reduced at all locations in cCSNB. However, the amplitude of the positive wave is relatively preserved in the central retina, and the relative amplitude of the positive wave to the a-wave became small from the center to the periphery. The changes in the waveforms were clearly seen when the responses were grouped for each eccentric rings (Fig. 3C). The remaining positive wave is well preserved in the central retina, but gradually became smaller towards the peripheral retina. The amplitude ratio of the positive wave to the a-wave was >1.0 in the central retina, but <1.0 in the periphery. These findings are consistent with our combined findings of full-field ERG and focal macular cone ERGs in patients with cCSNB.

We also confirmed these results in a monkey retina after treatment with APB (Fig. 4). The remaining positive response was relatively large in the central retina, but the relative ratio of the positive wave to the a-wave gradually became smaller towards the periphery (Fig. 4C). These findings were quite similar to those in patients with cCSNB.

3.4. Origin of the remaining positive wave of photopic ERG at central retina

One question that still remained was the origin of the remaining positive component of the focal macular cone ERG seen even after blockage of cone on-pathway. To study the retinal origin of this component, we added PDA to block the neural activities of post-synaptic off-pathways and horizontal cells in monkeys. Fig. 5 shows the changes in the waveforms of photopic ERG with long duration stimulus before and after APB and PDA application for full-field and focal macular cone ERGs in a rhesus monkey. In this experiment, the same stimulus (30 cd/m^2) and background (3 cd/m^2) intensities were used for both full-field and focal macular cone ERGs, because the waveform of photopic ERG is dependent on the stimulus and background intensities (Kondo et al., 2000; Ueno, Kondo, Niwa, Terasaki, & Miyake, 2004). We found that after the PDA injection, the remaining positive wave of focal macular cone ERGs completely disappeared (lower traces of Fig. 5).

4. Discussion

We compared the waveform of focal macular cone ERGs recorded from cCSNB patients with those from APB-treated monkeys, and found that the waveforms were very similar: the amplitude of the a-wave was normal or slightly larger than control; a positive wave was still present after the a-wave, and the amplitude of this positive wave was larger than that of the a-wave; and the implicit time of the positive wave was delayed. These similarities in the waveform of focal macular ERG between the cCSNB patients and APB-treated monkeys suggested that the cone on-pathway is nearly completely blocked even in the central retina of the cCSNB patients.

Although the waveform of the a-wave and the following positive wave were very similar for cCSNB patients and

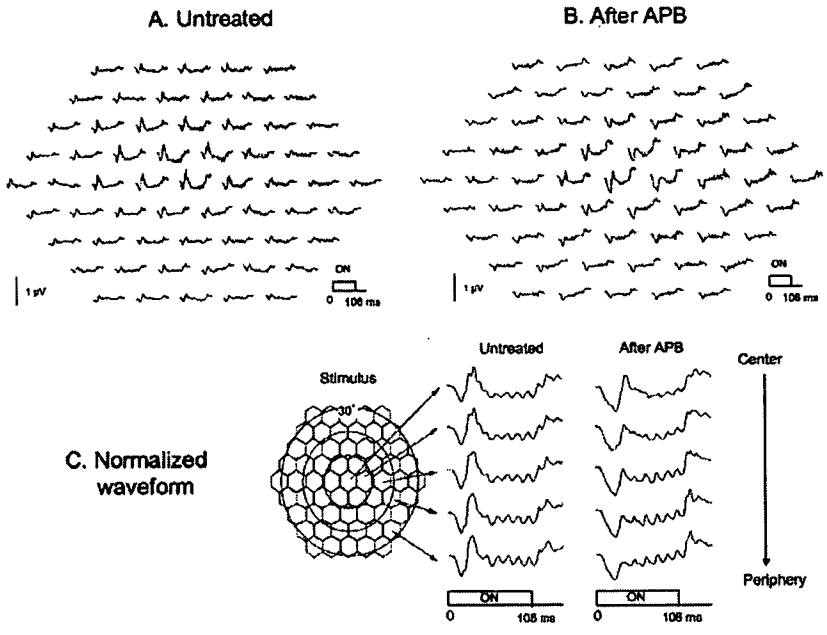

Fig. 4. Multifocal on- and off-responses before and after intravitreous injection of APB in a rhesus monkey. Intravitreous concentration of APB was 1.0 mM. Unstretched hexagonal elements (same size) are used for these monkey experiments. (A) Multifocal ERGs before APB. (B) Multifocal ERG after APB. (C) Normalized waveforms from five eccentric rings after APB application. The waveform after APB are very similar to those recorded from cCSNB patients.

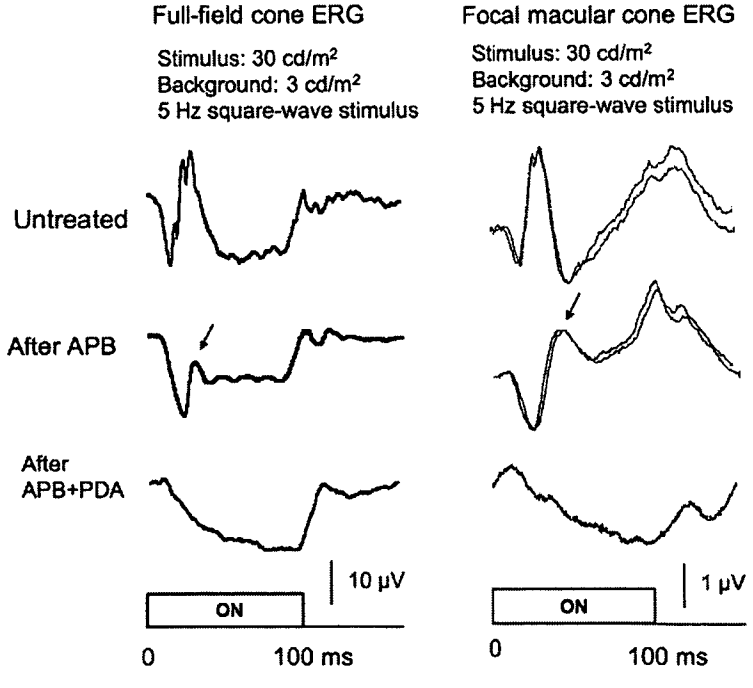

Fig. 5. Comparison in the waveforms of photopic ERG with long duration stimulus before and after APB and PDA application for full-field and focal macular cone ERGs in a rhesus monkey. Five hertz square-wave flickering stimulus of 30 cd/m^2 was presented on a background illumination of 3 cd/m^2 for both ERGs. After APB and PDA, the remaining positive wave at stimulus onset disappears completely for both ERGs (arrows).

APB-treated monkeys, the waveform of the d-wave at the offset of the stimulus was slightly different: the amplitude of the d-wave of the focal macular cone ERG was enhanced after the intravitreal injection of APB in monkeys, whereas the d-wave of focal macular cone ERG in cCSNB patients was not larger than that of myopic control. We do not know the reason for this difference in the waveform of the d-wave between the cCSNB patients and

APB-treated monkeys. However, it may be partly due to the differences between inherited human disease and the pharmacological animal model.

Although our electrophysiological study showed functional similarity between the retina of patients with cCSNB and APB-treated monkey retinas, there still remained the question of whether the retinal on-pathway is completely blocked in the retina of patients with cCSNB. Two psychophysical studies suggested that rod on-pathway may not be completely blocked in cCSNB patient (Allen et al., 2003; Young, Price, & Harrison, 1986).

We also found that even after a complete blockage of the cone on-pathway, there still remained a sizeable positive wave of the cone ERG in the central retina. The multifocal ERG results also demonstrated that the amplitude ratio of the positive wave to the a-wave was maximal in the central retina, and became gradually decreased towards the peripheral retina in a cCSNB patient and an APB-treated monkey supporting our combined findings of the full-field ERGs and focal macular cone ERGs. These results indicated that there is a unique spatial variation in the waveform of the cone ERGs. Other pharmacological studies in monkeys (Hare & Ton, 2002; Hood, Frishman, Saszik, & Viswanathan, 2002) also showed several spatial variations in the waveform of the cone ERGs using multifocal ERG technique, but they did not separate the on- and off-responses.

By adding PDA to APB, we found that the remaining positive wave of the cone ERG, which was seen even after blocking the cone on-pathway, originated from post-photoreceptor neurons which are sensitive to PDA, i.e., retinal neurons of the off-pathway or horizontal cells (Fig. 5). However, we could not identify exactly which retinal neurons/circuits contributed to this positive component. To identify the exact origin of this positive wave, further studies are needed using other pharmacological agents which affects specific retinal neurons.

Acknowledgments

The authors thank Laura J. Frishman of University of Huston for providing us her modified ophthalmoscope for multifocal ERG recordings for monkeys. We also thank Masao Yoshikawa, Eiichiro Nagasaka, Hidetaka Kudo of Mayo Corporation for technical helps.

References

Allen, L. E., Zito, I., Bradshaw, K., Patel, R. J., Bird, A. C., Fitzke, F., et al. (2003). Genotype-phenotype correlation in British families with X linked congenital stationary night blindness. *British Journal of Ophthalmology, 87*, 1413–1420.

Bech-Hansen, N. T., Naylor, M. J., Maybaum, T. A., Sparkes, R. L., Koop, B., Birch, D. G., et al. (2000). Mutations in NYX, encoding the leucine-rich proteoglycan nyctalopin, cause X-linked complete congenital stationary night blindness. *Nature Genetics, 26*, 319–323.

Dryja, T. P., McGee, T. L., Berson, E. L., Fishman, G. A., Sandberg, M. A., Alexander, K. R., et al. (2005). Night blindness and abnormal cone electroretinogram ON responses in patients with mutations in the GRM6 gene encoding mGluR6. *Proceedings of the National Academy of Sciences of the United States of America, 102*, 4884–4889.

Evers, H. U., & Gouras, P. (1986). Three cone mechanisms in the primate electroretinogram: Two with, one without OFF-center bipolar responses. *Vision Research, 26*, 245–254.

Hare, W. A., & Ton, H. (2002). Effects of APB, PDA, and TTX on ERG responses recorded using both multifocal and conventional methods in monkey. Effects of APB, PDA, and TTX on monkey ERG responses. *Documenta Ophthalmologica., 105*, 189–222.

Hood, D. C., Frishman, L. J., Saszik, S., & Viswanathan, S. (2002). Retinal origins of the primate multifocal ERG: Implications for the human response. *Investigative Ophthalmology & Visual Science, 43*, 1673–1685.

Houchin, K., Purple, R. L., & Wirtschafter, J. D. (1991). X-linked congenital stationary night blindness and depolarizing bipolar system dysfunction. [ARVO abstract]. *Investigative Ophthalmology & Visual Science, 32*, S1229 (Abstract No. 2741S).

Khan, N. W., Kondo, M., Hiriyanna, K. T., Jamison, J. A., Bush, R. A., & Sieving, P. A. (2005). Primate retinal signaling pathways: Suppressing ON-pathway activity in monkey with glutamate analogues mimics human CSNB1-NYX genetic night blindness. *Journal of Neurophysiology, 93*, 481–492.

Knapp, A. G., & Schiller, P. H. (1984). The contribution of on-bipolar cells to the electroretinogram of rabbits and monkeys. *Vision Research, 24*, 1841–1846.

Kondo, M., & Miyake, Y. (2000). Assessment of local cone on- and off-pathway function using multifocal ERG technique. *Documenta of Ophthalmologica, 100*, 139–154.

Kondo, M., Miyake, Y., Horiguchi, M., Suzuki, S., & Tanikawa, A. (1998). Recording multifocal electroretinogram on and off responses in humans. *Investigative Ophthalmology & Visual Science, 39*, 574–580.

Kondo, M., Miyake, Y., Kondo, N., Tanikawa, A., Suzuki, S., Horiguchi, M., et al. (2001). Multifocal ERG findings in complete type congenital stationary night blindness. *Investigative Ophthalmology & Visual Science, 42*, 1342–1348.

Kondo, M., Piao, C. H., Tanikawa, A., Horiguchi, M., Terasaki, H., & Miyake, Y. (2000). Amplitude decrease of photopic ERG b-wave at higher stimulus intensities in humans. *Japanese Journal of Ophthalmology, 44*, 20–28.

Leifert, D., Todorova, M. G., Prunte, C., & Palmowski-Wolfe, A. M. (2005). LED-generated multifocal ERG on- and off-responses in complete congenital stationary night blindness—A case report. *Documenta Ophthalmologica, 111*, 1–6.

Marmor, M. F., Hood, D. C., Keating, D., Kondo, M., Seeliger, M. W., & Miyake, Y. (2003). Guidelines for basic multifocal electroretinography (mfERG). *Documenta Ophthalmologica, 106*, 105–115.

Miyake, Y. (1988b). Studies of local macular ERG [in Japanese]. *Journal of Japanese Ophthalmological Society, 92*, 1418–1449.

Miyake, Y., Horiguchi, M., Suzuki, S., Kondo, M., & Tanikawa, A. (1997). Complete and incomplete type congenital stationary night blindness as a model of "OFF-retina" and "ON-retina". In M. M. LaVail, J. G. Hollyfield, & R. E. Anderson (Eds.), *Degenerative retinal diseases* (pp. 31–41). New York: Plenum Publishing.

Miyake, Y., Shiroyama, N., Ota, I., & Horiguchi, M. (1988a). Oscillatory potentials in electroretinograms of the human macular region. *Investigative Ophthalmology & Visual Science, 29*, 1631–1635.

Miyake, Y., Yagasaki, K., Horiguchi, M., & Kawase, Y. (1987). On- and off-responses in photopic electroretinogram in complete and incomplete types of congenital stationary night blindness. *Japanese Journal of Ophthalmology, 31*, 81–87.

Miyake, Y., Yagasaki, K., Horiguchi, M., Kawase, Y., & Kanda, T. (1986). Congenital stationary night blindness with negative electroretinogram: A new classification. *Archives of Ophthalmology, 104*, 1013–1020.

Pusch, C. M., Zeitz, C., Brandau, O., Pesch, K., Achatz, H., Feil, S., et al. (2000). The complete form of X-linked congenital stationary night blindness is caused by mutations in a gene encoding a leucine-rich repeat protein. *Nature Genetics, 26*, 324–327.

Rangaswamy, N. V., Hood, D. C., & Frishman, L. J. (2003). Regional variations in local contributions to the primate photopic flash ERG: Revealed using the slow-sequence mfERG. *Investigative Ophthalmology & Visual Science, 44*, 3233–3247.

Saeki, M., & Gouras, P. (1996). Cone ERGs to flash trains: The antagonism of a later flash. *Vision Research, 36*, 3229–3235.

Sieving, P. A., Murayama, K., & Naarendorp, F. (1994). Push-pull model of the primate photopic electroretinogram: a role for hyperpolarizing neurons in shaping the b-wave. *Visual Neuroscience, 11*, 519–532.

Terasaki, H., Miyake, Y., Nomura, R., Horiguchi, M., Suzuki, S., & Kondo, M. (1999). Blue-on-yellow perimetry in the complete type of congenital stationary night blindness. *Investigative Ophthalmology & Visual Science, 40*, 2761–2764.

Ueno, S., Kondo, M., Niwa, Y., Terasaki, H., & Miyake, Y. (2004). Luminance dependence of neural components that underlies the primate photopic electroretinogram. *Investigative Ophthalmology & Visual Science, 45*, 1033–1040.

Ueno, S., Kondo, M., Ueno, M., Miyata, K., Terasaki, H., & Miyake, Y. (2006). Contribution of retinal neurons to d-wave of primate photopic electroretinograms. *Vision Research, 46*, 658–664.

Young, R. S. L. (1991). Low-frequency component of the photopic ERG in patients with X-linked congenital stationary night blindness. *Clinical Vision Science, 6*, 309–315.

Young, R. S. L., Price, J., & Harrison, J. (1986). Psychophysical study of rod adaptation in patients with congenital stationary night blindness. *Clinical Vision Science, 1*, 137–143.

論　文

人工視覚を目指したCMOS LSI搭載フレキシブル網膜刺激デバイス

正　員　徳田　　崇*　　非会員　杉谷　幸愛*
非会員　浅野　良介*　　非会員　谷山　真理*
非会員　寺澤　靖雄**　　非会員　上原　昭宏**
非会員　香川景一郎*　　非会員　布下　正宏*
非会員　田野　保雄***　　非会員　太田　　淳*

A CMOS LSI-Based Flexible Retinal Stimulator for Retinal Prosthesis

Takashi Tokuda*, Member, Sachie Sugitani*, Non-member, Ryosuke Asano*, Non-member, Mari Taniyama*, Non-member,
Yasuo Terasawa**, Non-member, Akihiro Uehara**, Non-member, Keiichiro Kagawa*, Non-member,
Masahiro Nunoshita*, Non-member, Yasuo Tano***, Non-member, Jun Ohta*, Non-member

A CMOS LSI-based neural stimulator was developed for retinal prosthesis. The stimulator was designed with "multi-chip" architecture. Small LSI neural stimulators named "Unit Chip" were assembled on a flexible substrate into a flexible, multi-site retinal stimulator. An experimental system equipped with the fabricated LSI-based flexible stimulator was configured and current injection functionality was demonstrated in saline solution. Materials for improved charge injection were also discussed.

キーワード：ニューロインターフェイス，電気刺激，人工視覚
Keywords : neurointerface, electric stimulation, retinal prosthesis

1. 序　論

近年，LSIをはじめとするエレクトロニクスデバイスを積極的に生体・神経インターフェイスとして利用する研究が広がりを見せている[(1)~(4)]。エレクトロニクスデバイスによるバイオインターフェイス技術として期待されるものの一つに人工視覚技術がある[(5)~(11)]。いうまでもなく視覚は人間にとって最重要ともいえる感覚機能である。進行すると失明に至る可能性が高く，患者数の多い網膜色素変性および加齢性黄斑変性は，現在のところ医学的に治療が困難とされている。しかしこれらの眼疾患では，視細胞は死滅するものの，一部の網膜細胞層が生存しているとされる。網膜刺激型人工視覚技術は，残存する網膜細胞を直接電気的に刺激し，代替視覚を提供することを目的としている。現在，人工視覚の研究は主にポリイミドやパリレンといったフレキシブル薄膜基板に形成した電極アレイが用いられている。将来の実用化においては高解像度達成のためにLSIを用いた数百～千点以上の網膜刺激デバイスが必要になると考えられる。一方，単結晶半導体で作製されるSi LSIは，網膜刺激デバイスに実装するために薄く研磨すると容易に折損するようになる。我々は，Si LSIによる多点網膜刺激デバイスに屈曲性を付与しうる構造として，分散型アーキテクチャを提案した[(12)~(15)]。人工視覚向けの分散型アーキテクチャとは，小型（数百μm角）のCMOS LSI電気刺激チップ（単位チップ）をフレキシブル基板上に配列し，LSIチップへストレスをかけることなく屈曲可能な多電極刺激デバイスを実現するものである。我々はこれまでに，この分散型アーキテクチャに対応した単位チップを設計・試作し，これを3×4マトリクスに配列したフレキシブル網膜刺激デバイスを作製し，基礎特性を評価した。

本論文では，動物実験に適応した分散型アーキテクチャによる網膜刺激デバイスを試作した。新しいデバイス実装形態を導入することで屈曲性を向上し，直径10mm以下の眼球に適応することに成功した。また生理食塩水中で電流注入機能を評価した。さらに電流注入性能を向上させるた

* 奈良先端科学技術大学院大学 物質創成科学研究科
〒630-0192　奈良県生駒市高山町8916-5
Graduate School of Materials Science, Nara Institute of Science and Technology,
8916-5 Takayama, Ikoma, Nara, 630-0192
** (株)ニデック 人工視覚研究所
〒443-0036　愛知県蒲郡市浜町73-1
Vision Institute, NIDEK Co., Ltd.,
73-1 Hama, Gamagori, Aichi, 443-0036
*** 大阪大学大学院医学系研究科
〒565-0871 大阪府吹田市山田丘2-15
Graduate School of Medicine, Osaka University
2-15 Yamadaoka, Suita, Osaka 565-0871

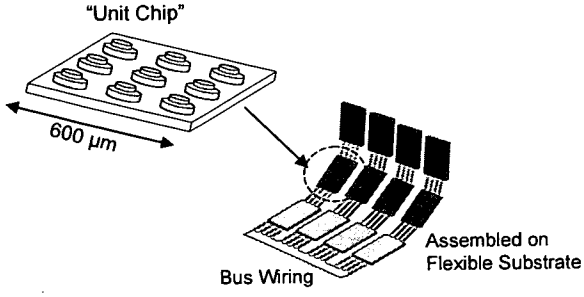

Fig. 1. Concept of multi-chip flexible stimulator

めに，IrOx および TiN 電極について評価・検討を行った。

2. 分散型アーキテクチャによる CMOS LSI 搭載フレキシブル網膜刺激デバイスの作製

〈2·1〉 分散型網膜刺激デバイスの概要 Figure 1 に，我々の提案する，LSI 搭載フレキシブル網膜刺激デバイス向け分散型アーキテクチャの概念を示す。電気刺激対象の生体組織等が湾曲している場合，刺激デバイスに屈曲性を付与する必要がある。一方で，限られた制御配線で高密度な電気刺激を実現するためには，LSI を用いたデマルチプレクサを搭載する必然性がある。分散型アーキテクチャにおいては，小型（本研究では 600μm×600μm）の多点電気刺激デバイスである単位チップを，適当なピッチ（1100μm）でフレキシブル基板上に実装する。この構造を採ることにより，単位チップの間の部分で屈曲することが可能となる。単位チップのサイズと配置間隔は，実験動物（ウサギ，ネコ等）の眼球直径（10-15mm 程度）および人間の眼球直径（24mm 前後）をカバーするように設定してある。単位チップの間の 500μm には電極を配置することができず，刺激イメージの欠落が懸念される。しかし現在の人工視覚において想定されている電極間隔は 100μm-500μm 程度であるため，技術の想定する機能の観点からは，単位チップ間の実装間隔 0.5mm は許容できると考えられる。

〈2·2〉 単位チップの構成と機能 本研究では，0.35μm ルール，2-poly 4-metal の標準 CMOS プロセスを用いて単位チップを設計・試作した。当該ルールでの標準電源電圧は 3.3V であるが，5V 耐圧仕様のトランジスタを用いて回路を設計し，5V 動作可能な回路とした。Figure 2 に，単位チップのブロックダイヤグラムとレイアウト（顕微鏡写真）を示す。単位チップは 17 個の接続パッドを備えており，このうち四隅，各辺の中央，およびチップ中央の 9 個が神経への刺激出力機能をもつ。そのほかの 8 個の接続パッドはチップの電源及び制御入力となっている。この単位チップは，VDD および GND の電源入力および，電極選択のためのディジタル入力である CONTROL，刺激電流の入力である STIM の 4 つの入力で動作する。多様な実装形態に対応するため，4 つの入力について 2 つずつ接続パッドを搭載しているが，現在の実装ではいずれか一方，合計で 4 つの入力配線を接続することで動作させる。単位チップ上の 9 個の電極には，それぞれ"0001"から"1001"までの 4 ビットのアドレスが割り当てられており，任意の電極を指定して STIM 入力と接続することができる。加えて，単位チップを指定するための 6 ビットのアドレス空間が設定されている。単位チップには，設計時に 6 ビットの固有の ID が組み込まれており，6+4=10 ビットのアドレスにより，一組の入力配線に接続された最大 64 個の単位チップ上の任意の電極を指定することができる。単位チップの ID は LSI 製造後でもレーザリペアプロセスによりアドレス変更用ヒューズを切断することで変更できる。

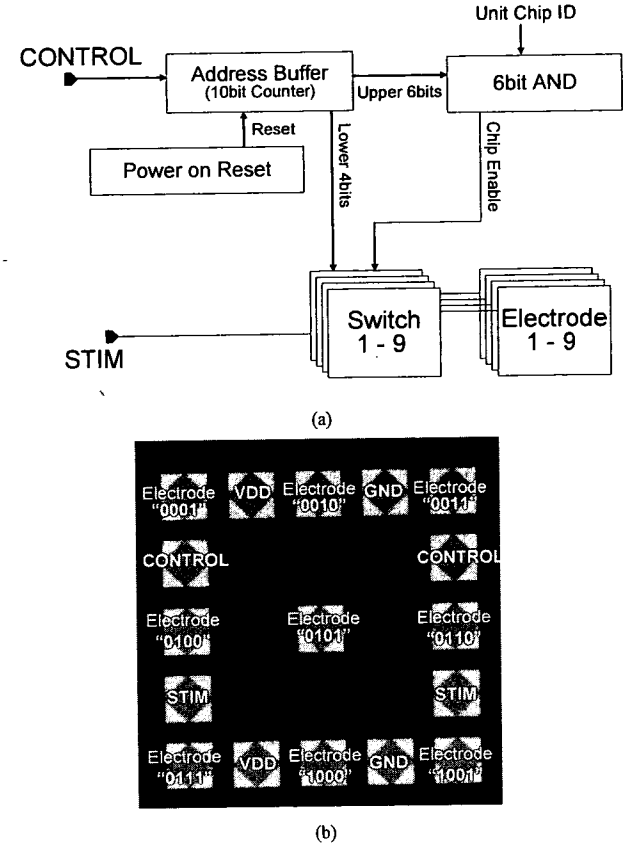

Fig. 2. (a)Block diagram and (b)layout of the unit chip

各単位チップは 10 ビット非同期カウンタをアドレスバッファとして備えている。単位チップおよび電極を指定するためのアドレスは，CONTROL 入力に与えられるディジタルパルスの数で指定する。各単位チップは上位 6 ビットとチップ ID が一致した場合にのみ下位 4 ビットで指定される電極と STIM 入力を接続する。接続は，並列接続された NMOS および PMOS スイッチによって構成されるトランスミッションゲート回路とした。また，同じ配線に接続された単位チップ間のアドレスの同一性を保障するため，電源投入後一定時間してからアドレスをリセットする，パワーオンリセット回路を搭載した。

Figure 2(a) に示すように，単位チップは刺激電極選択のためのディジタル回路およびアナログスイッチ回路で構成され，刺激電流発生回路をもたない。さらに動作時間の大半を占める電気刺激動作中には CMOS ディジタル回路には状態変化が生じないためほとんど電力を消費しない。この

結果，VDD から供給されてチップ上で消費される電力は，STIM からの刺激電流がスイッチ回路（オン抵抗 100Ω-200Ω）を流れることによって消費される電力に比べて無視できる。単位チップ上での最大の電力消費要素であるスイッチ回路の消費電力は，たとえば本デバイス設計時に想定した標準的な電気刺激条件（500μA, 500μs, バイフェージック, 100Hz）で最大 10mW となる。

〈2･3〉 フレキシブル網膜刺激デバイスの実装プロセス

提案する網膜刺激デバイスの実現のためには，実装技術もきわめて重要である。LSI の正常な動作のためには，刺激電極以外は生体環境から防水・絶縁しなければならない。LSI の接続パッドとして標準的な Al は，生体適合性，電流注入性能，耐腐食性のいずれにおいても生体刺激電極としての条件を満たさない。我々は，純金属として最も生体刺激電極として優れているとされる Pt を搭載した実装を報告した[12)~15)]。今回，この実装技術をベースとし，さらに動物実験に向けたサイズの適正化と屈曲性の向上を達成した。

人工視覚における動物実験には，検討内容に応じてウサギ，ネコなどが用いられる。いずれの動物も眼球の直径は 10-15mm 程度であり，従来報告した人間の眼球サイズ（直径 24mm 程度）へ適応した屈曲性では不十分であった。これまでの実装では，ポリイミドフレキシブル基板を中心に，上下にフィルムを張り合わせた形状となっているため，屈曲性に限界があった。そこで今回，フリップ実装の後に，あらかじめ LSI チップ上に形成した Au バンプを露出させ，この上に Pt バンプ電極を形成する方法を採った。また従来は LSI の分割方法として，チップ表面から溝を形成，裏面から研磨して単位チップ同士を分割するプロセス (Dice Before Grinding, DBG) を用いていた。このプロセスのメリットは，表面から分離位置をパターニングできることによるアラインメントの正確さであったが，フリップチップ実装時に溝に充填されてしまう包埋樹脂の完全な除去が困難であり，完成後の屈曲性能を制限していた。そこで，裏面から単位チップの場所にあわせてエッチングを行うプロセスを開発した。これらを導入した新しい実装プロセスの概要を以下に述べる (Figure 3)。なお本研究では，実装を容易にするため，異なる ID をもつ単位チップを 4×4 配列で一つの Si チップ上に並べて設計している。また，実装前の LSI の厚さは 150μm である。

① LSI 上への Au バンプの形成

単位チップの接続パッド上に，ボール/バンプボンダ (WESTBOND Model 7700) を用いて Au バンプを形成する。この際，9 個の電気刺激用パッドには先端を平坦化した Au バンプを，4 つの信号入力用のパッドには平坦化しない Au バンプを形成する。

② フリップチップボンディング

LSI チップをポリイミドフレキシブル基板へフリップチップボンディングする。この時点で 4 本の信号入力へ配線が接合される。フリップチップボンディングにおいては LSI チップとフレキシブル基板の間にエポキシ樹脂を充填し，接合強度を確保する。

③ 単位チップ分離

深堀り反応性イオンエッチング (Deep Reactive Ion Etching, Deep RIE) プロセスを用いて，裏面より単位チップを分離する。エッチングのマスクとしては Al 蒸着膜（厚さ 200nm）を用いる。

④ 裏面包埋

7.5μm 厚テフロンフィルムを裏打ちフィルムとし，LSI の包埋を行う。包埋の際にはジグを用いて，単位チップ間の包埋樹脂を押し出し，屈曲性を確保する。包埋樹脂としては，テフロンに対してある程度の密着性を示すポリエステル系熱可塑性樹脂を用いている。テフロンフィルムが薄いため，接着時のジグでの圧迫によって単位チップの形状に沿わせて成型でき，屈曲性改善に寄与している。

⑤ Pt 刺激電極の形成

ポリイミドフレキシブル基板に開口を形成し，ステップ①で単位チップ上に形成した平坦化 Au バンプを露出させる。露出した Au バンプ上に，Au バンプ形成時と同じボール/バンプボンダによって Pt バンプを形成し，神経刺激電極とする。形成した Pt 電極の先端部は平坦化し，電極周辺を樹脂包埋する。Pt 電極露出部の直径は 90±10μm である。

⑥ 外周加工

レーザ加工技術により，デバイス外形を形成する。この段階で不要なチップは切り落とされ，所望のデバイス形状を得る。

Figure 4 に，実際に作製した，動物実験向け 1×4 配列網膜刺激デバイスの写真を示す。Figure 4 にみられるように，曲率半径 10mm 以下の屈曲性を達成した。

本デバイスは，動物を用いた急性の網膜刺激を目的としており，網膜下（網膜と，その外側の脈絡膜の間），もしくは眼球最外部の強膜に形成したポケット構造へ埋植して用いる。いずれも，デバイス幅に合わせて形成した組織の剥離部に差し込む形態となり，縫合糸を用いて挿入位置でデ

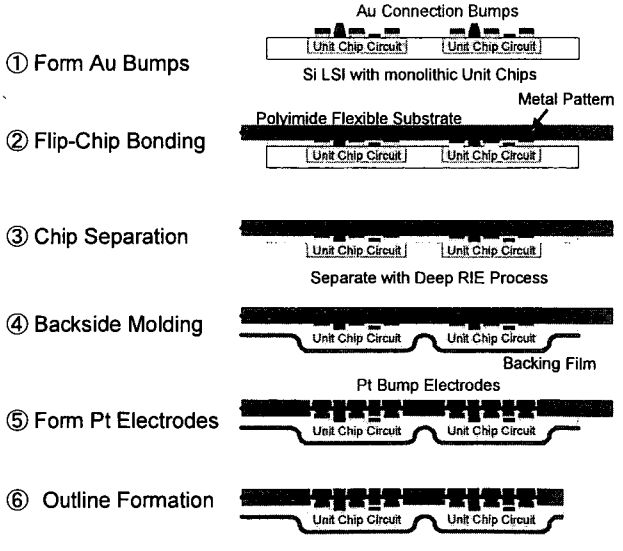

Fig. 3. Assemble process for multi-chip flexible stimulator

バイス（基板部）を組織に縛りつけ，実験期間内で安定した固定を実現する。

〈2·4〉 動物実験用電気刺激システムおよび安全な電気刺激のための動作 本デバイスを用いた生体神経の刺激においては，デバイス本体のほかに，刺激電極から流した電流を回収する対向電極が必要となる。生体系と電気刺激系の相対電位を規定するために，対向電極の電位 Vref は刺激デバイスの駆動にあわせて適切に制御しなければならない。神経系への継続的な電気刺激を行う場合，生体への安全性の観点から，電荷バランスのとれた正負 2 つの電流パルスをセットで用いるバイフェージック刺激が現実的である。正負両極性の電流を流すためには，刺激電極の電位は対向電極の電位付近で上下に推移する必要がある。すなわちデバイスの動作時には，対向電極の電位は単位チップの動作電圧範囲の中央 (2.5V) 付近に維持する必要がある。一方，刺激デバイスが動作していない状態では，刺激電極の電位は GND レベルとなる。デバイス非動作時に想定外の電流が流れないようにするためには，デバイス非動作時には対向電極を外部制御回路によって刺激チップの GND レベルと短絡しなければならない。対向電極の電位制御を含め，安全な電流注入を実現するための外部システムおよびソフトウェアを開発した。Figure 5 に，外部制御システムの概要を示す。外部制御回路には，以下の機能を搭載した。

① 刺激デバイス・対向電極系を，外部電源および PC から電気的に絶縁。
② 対向電極の刺激デバイスに対する相対電位を，刺激デバイス非起動時には GND に，刺激デバイス動作時には任意の電位（標準は 2.5V）に維持。
③ 外部ファンクションジェネレータからの入力を刺激電流に変換。

Figure 5 のシステムにより，刺激デバイス系への電源の供給，アドレス指定の後，電流注入を自動的に行うことができる。また，チップの停止時には対向電極の電位を自動的に GND に短絡することにより，電気刺激デバイスの状態にかかわらず刺激対象の生体組織の安全性を向上させている。

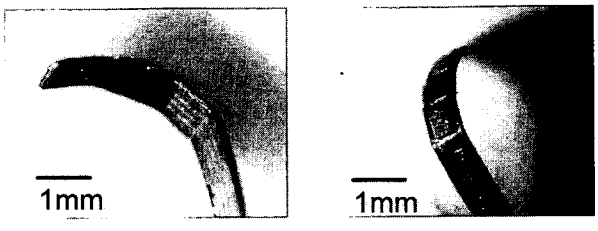

Fig. 4. Micrograph of the multi-chip flexible stimulator

3. フレキシブル網膜刺激デバイスの機能実証

〈3·1〉 網膜刺激デバイス系の動作シーケンス 本実験で試作したデバイスを生理食塩水中に浸漬し，バイフェージック電流注入動作を検証した。Figure 6 に，各信号の推移を示す。デバイス停止状態においては，対向電極の電位

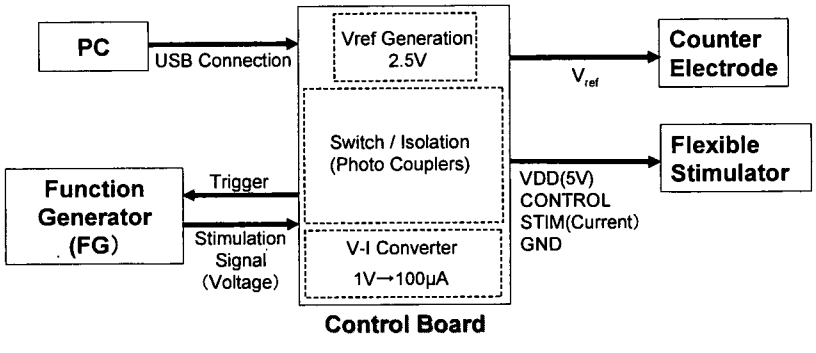

Fig. 5. Configuration of the experimental neural stimulation system

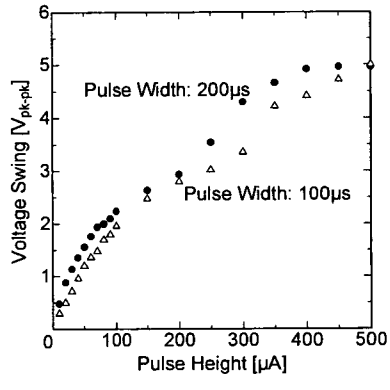

Fig. 7. Voltage swing in biphasic current injection

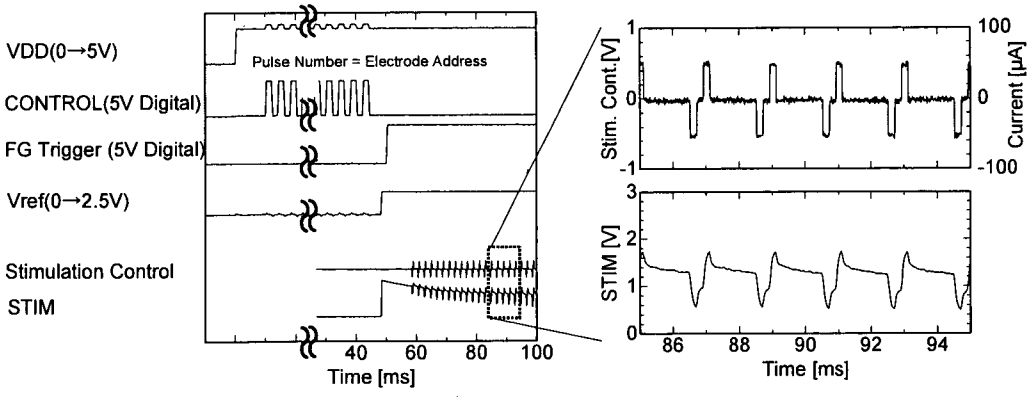

Fig. 6. Control sequence of the fabricated neural stimulation system

を含むすべての電位は0Vに維持される。デバイスの起動に先立ち，FGから制御ボックスへ入力する電圧信号は0を維持し，刺激デバイスの起動に伴って電極が選択されても意図しない電流が流れないように準備する。FGからの制御信号はPC制御されるトリガ信号によって，電極選択後に供給されるように設定しておく。

制御PC上で電極を指定し，デバイスの動作を開始すると，最初にVDD入力に5Vが供給され，各単位チップが動作開始する。パワーオンリセット回路の働きにより，起動時にはアドレス"000000000"が指定され，どの電極も選択されていない状態になる。次に，STIM入力に指定した電極に応じた数のディジタルパルスが入力され，電極が選択される。その後，対向電極の電位が指定電位（Figure 6では2.5V）にプルアップされる。これらの動作が完了した時点で，STIMラインの電位は，電流が流れない状態を維持しようとする刺激回路の働きにより，1.0～2.0V付近に上昇する。対抗電極，刺激電極ともにPtであるため電解液に対する電位は不安定とされるが，実際に注入を行うと我々のシステムでは電極の中立電位は1.1V付近で安定する。その後FGに対してトリガ信号が与えられ，FGが刺激電流を規定する信号を供給し，電流注入が開始される。指定されたバイフェージック電流注入を実現するために，STIM入力の電位は刺激回路によって自動的に制御され，両極性の電位推移を示す。現在の装置構成では制御信号と刺激電流の変換比は50μA/Vであり，Figure 6の例では，50μA/200μsの負電流パルスと50μA/200μsの正電流パルスが，200μsのパルス間インターバルで注入されている。

〈3·2〉 生理食塩水中での電流注入能力 電解液中に浸漬した金属電極からの電流注入には，電極表面での電気化学反応を伴う。その際，電気分解をはじめとする不可逆反応が生じてしまうと，電極の急速な腐食や生体組織の破壊などが生じる。電流注入を安全に行うためには，電極材料固有の安全な電圧範囲（電位窓）の中に収める必要がある。Ptを用いて電流を注入する際の安全電圧振幅は，1.65V（−0.6V～+1.05V vs Ag/AgCl）程度であると報告されている[16][17]。この電圧範囲は，単位チップの動作電圧範囲である5Vより十分小さいため，本刺激デバイスを用いた場合の電荷注入能力は，電極の材料及びサイズで決定される。Figure 7に，パルス幅，パルス間インターバル共に100μsおよび200μsの対称バイフェージック電流注入を行った際に生じたSTIM端子の電圧スイングをプロットする。Figure 7より，安全に電流注入できる，すなわち電圧スイングが1.65V以下である条件はパルス幅100μsでは70μA，パルス幅200μsでは50μA程度であると考えられる。この値は人工視覚研究において報告されている刺激閾値と比較すると1桁程度小さく，現状の装置の刺激機能には改善の余地があることがわかった。

4. IrOxおよびTiN電極による電荷注入性能の向上

前章において，本試作デバイスによりバイフェージック電気刺激が可能であることが確認したが，注入可能な電流は不足していることがわかった。本デバイスの電流注入能力を規定しているのは電極材料とサイズである。Ptは純金属としては，生体適合性と電荷注入能力のバランスのとれた最有力材料であるが，さらに優れた性能をもつとされる化合物電極の導入について検討を行った。人工視覚向け化合物電極材料として，IrOxおよびTiNが有力とされる。IrOx電極では，Irの酸化数が+3と+4の状態間で可逆的に遷移するため，Ptより大幅に大きな電荷注入能力を示す。一方，TiNは成膜条件によって表面の凹凸が増大し，実効的な表面積が増大し，純金属電極と比較して大きな電荷注入能力を示すとされる。純金属であるPtにおいても，白金黒（Pt black）という形態がしられており，表面のフラクタル構造によって生体計測・刺激電極としての特性に優れるが，機械的強度の面から人工視覚には適さない。本研究ではスパッタリング法によってIrOxおよびTiN膜を成膜し，電荷注入能力および1時間の生理食塩水中での連続通電（正負とも350μA/200μs，パルス間インターバル200μsのバイフェージック注入）に対する表面変化の有無を測定した。Table 1に，成膜条件と電極特性の関係を示す。電荷注入能力は，ま電流値・パルス幅を変化させ，安全とされる電圧範囲に収まっていた最大注入条件を単位面積あたりの電荷量で示した。また表面の変化（Table 1中ではPhysical Strength）は，上述の1時間連続通電後の表面状態を，○：変化なし，△：わずかに変化，×：明確なダメージを確認，の3段階で示した。TiNおよびIrOxでは電荷注入能力および膜強度は成膜条件に強く依存する傾向がみられた。電荷注入能力は最大で2800μC/cm^{2}程度と非常に大きな値を示した。しかし電荷注入能力と耐久性には強い負の相関があり，電荷注入能力に優れた膜は同時に強度が低かった。これは電流注入の際にIrの価数が変化し，原子レベルでの形状変化が繰り返され，膜の破損につながるものと考えられる。一方，TiNの特性はIrOxと比較すると成膜条件依存性は小さかった。IrOx膜，TiN膜において1時間の連続通電に耐えうる強度をもつものの電荷注入能力は300～800μC/cm^{2}および800～1600μC/cm^{2}程度であり，Ptの数倍に相当する。TiNおよびIrOxの成膜条件のさらなる最適化余地は残すものの，現状ではPt電極と同じ面積のTiNやIrOxの導入だけでは目標とする電極性能には達しない。そのため，TiNあるいはIrOx電極の導入とあわせて電極の大口径化も行う必要がある。Figure 8に，本研究で試作したフレキシブル網膜刺激デバイス上に形成したTiN電極膜（Table 1条件8）の写真を示す。成膜時にメタルマスクを用いて電極形状をパターニングしており，直径150μmの円形膜状電極の形成に成功している。最初に形成したPt電極の直径が90μm程度であるため，電極面積の2倍程度の拡大は比較的容易に達成できることがわかった。TiNの導入に加えて電極の大面積化を行うことにより，おおむね想定条件での電流注入動作の目処が立った。今後，IrOxおよびTiN電極を搭載したフレキシブル網膜刺激デバイスの性能確認および，これを用いた動物実験を行

Table 1. Sputtering conditions and characteristics of IrOx and TiN film electrode

Sample	Material	Pressure (Pa)	N_2 (Pa)	Ar (Pa)	O_2 (Pa)	Discharge	Injection Capability ($\mu C/cm^2$)	Physical Strength
1	IrOx	0.2	0	0.16	0.04	RF200W	350-1200	×
2	IrOx	1.0	0	0.8	0.2	RF200W	300-800	○
3	IrOx	1.0	0	0	1	RF200W	600-1700	×
4	IrOx	10	0	8	2	RF200W	1800-2800	×
5	TiN	0.4	0.15	0.25	0	DC500W	～100	×
6	TiN	1.0	0.55	0.45	0	DC500W	400-600	○
7	TiN	1.0	0.38	0.62	0	DC500W	200-600	○
8	TiN	5.0	2.7	2.3	0	DC500W	800-1600	○
9	TiN	5.0	1.9	3.1	0	DC500W	～100	△
10	Pt	0.6	0	0.6	0	RF500W	100-200	○

Fig. 8. TiN electrodes formed on the flexible stimulator

っていく予定である。

5. 結　論

人工視覚を目指した，CMOS LSI 搭載型フレキシブル人工視覚デバイスを試作・評価した。小型の電気刺激チップをフレキシブル基板上に実装することにより，LSI による多点刺激機能と屈曲性を両立した。動物実験に対応するためのデバイス構造および実装技術の開発を行い，直径 10mm に対応する屈曲を実現した。試作したフレキシブル網膜刺激デバイスおよび対向電極を安全に駆動するための制御システムを構築し，生理食塩水中での電流注入実験に動作に成功した。また，電荷注入能力を向上させるための電極材料について検討を行い，IrOx および TiN 薄膜電極の成膜条件の最適化を行った。

一方で，本稿において実現した網膜刺激デバイスは急性の動物実験を目指したものであり，長期埋植を行った場合の防水性の維持や生体への影響の有無は未検討である。また，電極性能は想定条件に対してほとんどマージンがなく，耐久性も高くない。これら，①包埋性能の向上，②生体適合性の向上，③電極性能と耐久性の確保，の 3 点は，今後想定される長期埋植しての動物実験，さらには人間への適用に向けての最大の技術課題となる。

謝　辞

本研究は NEDO 次世代戦力技術実用化開発助成事業および厚生科研費により行われた。

（平成 19 年 2 月 5 日受付，平成 19 年 5 月 16 日再受付）

文　献

(1) K. Najafi and K. D. Wise : IEEE J. Solid-State Circuits, Vol.21, p.1035 (1986)
(2) J. Ji, K. Najafi, and K. D. Wise : IEEE Trans. Biomed. Eng., Vol.38, p.75 (1991)
(3) T. Kawano, Y. Kato, R. Tani, H. Takao, K. Sawada, and M. Ishida : IEEE Trans. Electron Devices, Vol.51, p.415 (2004)
(4) B. Eversmann, M. Jenkner, F. Hofmann, C. Paulus, R. Brederlow, B. Holzapfl, P. Fromherz, M. Merz, M. Brenner, M. Schreiter, R. Gabl, K. Plehnert, M. Steinhauser, G. Eckstein, D. S.-Landsiedel, and R. Thewes : IEEE J. Solid-State Sircuits, Vol.38, p.2306 (2003)
(5) E. Margalit, J. D. Weiland, R. E. Clatterbuck, G. Y. Fujii, M. Maia, M. Tameesh, G. Torres, S. A. D'Anna, S. Desai, D. V. Piyathaisere, A. Olivi, E. de Juan, and M. S. Humayun : J. Neurosci. Methods, Vol.123, p.129 (2003)
(6) W. Liu, K. Vichienchom, M. Clements, S. C. DeMarco, C. Hughes, E. McGucken, M. S. Humayun, E. de Juan, J. D. Weiland, and R. Greenberg : IEEE J. Solid-State Circuits, Vol.35, p.1487 (2000)
(7) S. C. DeMarco, W. Liu, P. R. Singh, G. Lazzi, M. S. Humayun, and J. D. Weiland : IEEE J. Solid-State Circuits, Vol.38, p.1679 (2003)
(8) J. Ohta, N. Yoshida, K. Kagawa, and M. Nunoshita : J. Jpn. Appl. Phys., Vol.41, p.2322 (2002)
(9) K. Kagawa, K. Isakari, T. Furumiya, A. Uehara, T. Tokuda, J. Ohta, and M. Nunoshita : Electron. Lett., Vol.39, p.419 (2003)
(10) H. Kanda, T. Morimoto, T. Fujikado, Y. Tano, Y. Fukuda, and H. Sawai, Invest. Ophthal. & Vis. Sci., Vol.45, p.560 (2004)
(11) K. Nakauchi, T. Fujikado, H. Kanda, T. Morimoto, J.S. Choi, Y. Ikuno, H. Sakaguchi, M. Kamei, M. Ohji, T. Yagi, S. Nishimura, H. Sawai, Y. Fukuda, and Y. Tano : Graefes Arch. Clin. Exp. Ophthalmol., Vol.243,

p.169 (2005)
(12) Yi-Li Pan, T. Tokuda, A. Uehara, K. Kagawa, M. Nunoshita, and J. Ohta : Jpn. J. Appl. Phys, Vol.44, p.2099 (2005)
(13) T. Tokuda, Yi-Li Pan, A. Uehara, K. Kagawa, M. Nunoshita, and J. Ohta,, Sensors and Actuators A, Vol.122, p.88 (2005)
(14) J. Ohta, T. Tokuda, K. Kagawa, T. Furumiya, A. Uehara, Y. Terasawa, M. Ozawa, T. Fujikado, and Y. Tano : IEEE Engineering in Medicine and Biology Magazine, Vol.25, p.47 (2006)
(15) T. Tokuda S. Sugitani, M. Taniyama, A. Uehara, Y. Terasawa, K. Kagawa, M. Nunoshita, Y. Tano, and J. Ohta : Jpn. J. Appl. Phys., in press.
(16) T. L. Rose and L. S. Robblee : IEEE Trans. Biomed. Eng., Vol.37, p.1118 (1990)
(17) S. B. Brummer and M. J. Turner : IEEE Trans. Biomed. Eng., Vol.24, p.440 (1977)

徳田　崇

（正員）　1998年3月京都大学大学院工学研究科博士後期課程修了。同年4月より日本学術振興会特別研究員 (PD)。1999年4月より奈良先端科学技術大学院大学物質創成科学研究科助手。半導体フォトニクスデバイス，特にバイオイメージングデバイス，ニューロエレクトロニクスデバイスの研究に従事。博士（工学）。

杉谷幸愛

（非会員）2005年3月筑波大学第一学群自然学類卒業，同年4月より奈良先端科学技術大学院大学 物質創成科学研究科修士課程。人工視覚の研究に従事。

浅野良介

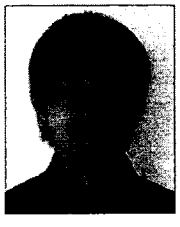

（非会員）2006年3月三重大学工学部物理工学科卒業，同年4月より奈良先端科学技術大学院大学物質創成科学研究科修士課程。LSIを搭載した人工視覚デバイスの研究に従事。

谷山真理

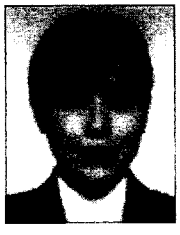

（非会員）2005年3月日本大学理工学部航空宇宙工学科卒業，同年4月より奈良先端科学技術大学院大学物質創成科学研究科修士課程。LSIを用いた人工視覚デバイスの研究に従事。

寺澤靖雄

（非会員）1998年3月東北大学大学院情報科学研究科博士前期課程修了。2001年（株）ニデック人工視覚研究所研究員。医用生体工学，特に人工視覚システムの研究開発に従事。修士（工学）。

上原昭宏

（非会員）　1997年3月大阪大学工学部卒業，2000年奈良先端科学技術大学院大学物質創成科学研究科博士前期課程修了。2002年（株）ニデック入社。人工視覚デバイスおよびシステムの研究開発に従事。2005年3月奈良先端科学技術大学院大学博士後期課程修了。博士（工学）。

香川景一郎

（非会員）2001年，大阪大学大学院工学研究科博士後期課程修了。光コンピューティングの研究に従事。同年，奈良先端科学技術大学院大学物質創成科学研究科助手。現在，ビジョンチップおよびその応用システムの研究に従事。博士（工学）。

布下正宏

（非会員）1967年3月大阪大学大学院基礎工学研究科修士課程修了。同年4月三菱電機（株）に入社。光機能デバイス，半導体デバイス，表示デバイスの研究開発と事業化に従事。1998年，奈良先端科学技術大学院大学物質創成科学研究科教授。工学博士。

田野保雄

（非会員）　1972年3月大阪大学医学部卒業。同年7月大阪大学医学部附属病院眼科勤務，1974年1月松山赤十字病院眼科勤務。1975年3月より大阪大学医学部眼科助手，1981年講師，1985年眼科医長を経て1991年9月より大阪大学医学部眼科教授。大阪大学医学部付属病院副病院長（併任）。日本眼科学会理事長。医師，医学博士。

太田　淳

（非会員）1983年3月東京大学大学院工学研究科修士課程修了。同年4月三菱電機（株）入社。1992～1993年，コロラド大学客員研究員。1998年4月より奈良先端科学技術大学院大学物質創成科学研究科助教授。2004年同大学教授。ビジョンチップおよびフォトニクスデバイスの研究に従事。博士（工学）。